ORIGINAL RESEARCH Open access

Explainable Machine Learning for Predicting Soil Nitrogen, Phosphorus, and Potassium in Cabbage Cultivation

Kristian Eriksen[1*], Solveig Berg[1]

Abstract

Cabbage (*Brassica oleracea* var. *capitata*) is a crop predominantly grown in elevated terrains, producing heads with tightly clustered foliage. Among its cultivars, Green Coronet stands out for its vigorous development and broad culinary applications. Attaining maximum productivity is fundamental to food security. Reliable estimation of the principal soil macronutrients—namely nitrogen, phosphorus, and potassium—is critical for yield optimization. Artificial intelligence techniques are increasingly deployed for nonlinear forecasting tasks that require interpretability. This investigation examined the capacity of explainable machine learning approaches to estimate soil nitrogen, phosphorus, and potassium concentrations over an 85-day cabbage-growing cycle. The study was performed on cabbage specimens cultivated in Sri Lanka's central highlands. The model's outputs were interpreted using SHapley Additive exPlanations (SHAP) and Local Interpretable Model-agnostic Explanations (LIME). According to SHAP assessments, elevated feature magnitudes for days elapsed and mean leaf surface area exerted a detrimental influence on nutrient forecasts. In contrast, higher leaf quantity and plant stature contributed favorably. Verification involved selecting 15 greenhouse-raised cabbage plants at distinct developmental phases. Actual nitrogen, phosphorus, and potassium readings were obtained and cross-referenced against the model's projections. These revelations help sharpen predictive frameworks and streamline agronomic procedures. An intuitive digital interface was engineered to facilitate user access to and comprehension of the model's forecasts. This platform delivers a straightforward experience for stakeholders, empowering them to harness the model's predictive power efficiently.

Keywords Cabbage, Deep neural network, Explainable machine learning, Major soil nutrients, Plant growth characteristics

*Correspondence:
Kristian Eriksen
kristian.eriksen@ntnu.no
[1] Department of AI for Precision Forestry and Timber Yield Prediction, Faculty of Environmental Sciences, Norwegian University of Science and Technology, Trondheim, Norway

Introduction

Cabbage (*Brassica oleracea* var. *capitata*) is a biennial crop known for its firm, layered heads. Classified within the Brassicaceae lineage [1, 2], it shares ancestry with broccoli, cauliflower, and Brussels sprouts. Domesticated through millennia, cabbage enjoys worldwide appreciation for both its gastronomic flexibility and its health-promoting properties [3]. From a nutritional standpoint, cabbage offers a low-calorie, nearly fat-free profile, along with indispensable micronutrients [4, 5]. It serves as an abundant reservoir of vitamin C (reaching concentrations up to 53.32 mg/100 g), bolstering immune defense and protection against oxidative stress [6]. Furthermore, it delivers substantial vitamin K necessary for hemostasis and skeletal integrity, supplies roughage for digestive tract maintenance, and provides a spectrum of B-complex vitamins (folate, pantothenic acid, pyridoxine) together with vital minerals (potassium, manganese), contributing to a comprehensive dietary intake [1, 7]. A wide array of cabbage varieties is cultivated

This is an open access article distributed under the terms of the Creative Commons Attribution-NonCommercial-ShareAlike 4.0 International License (CC BY-NC-SA 4.0), which permits non-commercial use, distribution, reproduction, and adaptation in any medium or format, provided that appropriate credit is given to the original author(s) and source, a link to the license is provided, and any changes made are indicated. Adapted material must be distributed under the same license.

© 2022 The Author(s). | Published by Agro Intelligence Research Press

worldwide. Napa cabbage (Pe-tsai group) presents elongated, supple foliage ideal for wraps and the fermentation of kimchi [8]. Savoy cabbage (Capitata group) is characterized by puckered, loosely arranged leaves, typically used in soups and baked dishes due to their moisture-retentive qualities [9]. Bok choy (Chinensis group) has sturdy petioles and dark, emerald blades, commonly used in quick-fried dishes and clear soups [10]. Lastly, Brussels sprouts (Gemmifera group) develop diminutive, cabbage-like buds along erect stalks, offering a distinctive flavor profile suited to oven-roasting and steaming [11].

Nutrient supplementation stands as a cornerstone of successful cabbage husbandry [12]. Like other botanical species, cabbage requires ample availability of the three foundational macronutrients—nitrogen (N), phosphorus (P), and potassium (K)—to sustain its physiological functions and biomass accumulation [1, 13, 14]. In mainstream production systems, growers typically apply synthetic fertilizer formulations containing urea, muriate of potash, and triple superphosphate to meet these elemental requirements [15]. Conversely, ecologically oriented cultivation relies upon organic amendments including rice bran, poultry litter, bovine urine, cattle manure, and wood ash [16]. Irrespective of the adopted management philosophy, precise quantification of indigenous soil fertility is an indispensable preliminary step. Predictive analytical tools equip producers with actionable intelligence, permitting the design of site- and crop-specific nutrient management regimes.

Artificial Intelligence (AI)-enabled precision farming is fundamentally reshaping contemporary agricultural operations [17]. Machine learning architectures, instructed on comprehensive repositories spanning meteorological variables [18], edaphic attributes [1, 18, 19], archival productivity records [18, 20], and remotely captured spectral imagery [21-23], have matured to perform nuanced agricultural prognostications. Earlier scientific inquiries have rigorously probed the phytoextraction of heavy metals by Chinese cabbage (*Brassica chinensis* L.) propagated in substrates contaminated with cadmium (Cd), copper (Cu), nickel (Ni), lead (Pb), and zinc (Zn). Empirical evidence affirms that the phytoavailability and resultant tissue sequestration of these metallic elements are modulated by edaphic characteristics, most notably the hydrogen ion concentration. Specifically, one investigation found that the assimilation of Cd, Pb, and Zn into Chinese cabbage tissues is substantially governed by substrate pH, with higher acidity promoting metal solubilization and consequent plant uptake [24]. Concurrently, the speciation of these elements within the soil matrix governs their biological uptake. Cutting-edge computational frameworks have been deployed to refine predictions surrounding metal translocation in Chinese cabbage. A particularly innovative methodology fuses Geographic Information System layers with deep learning architectures to project harvest outcomes as a function of terrain properties. To illustrate, an adapted Convolutional Neural Network-Recurrent Neural Network hybrid was engineered to estimate cabbage productivity by distilling pedological signatures from SoilGrids databases and land suitability cartography. This analytical construct effectively captures the multifaceted interdependencies between soil parameters and agronomic performance [25]. In parallel, deep neural architectures have been trained to infer soil nitrogen, phosphorus, and potassium status from observable cabbage phenotypic traits. By scrutinizing diverse vegetative growth indices, these computational systems can reliably back-calculate rhizosphere nutrient concentrations, thus reinforcing the principles of precision agriculture. Such prognostic competencies prove invaluable for tailoring fertilization interventions and safeguarding long-term agrarian output [1]. Regrettably, a concomitant erosion of operational transparency has occurred, leaving agricultural practitioners unable to decipher the mechanistic logic behind algorithmic outputs or to gauge the directional influence of input variables [26, 27]. The discipline of Explainable AI demystifies predictive processes by articulating the contribution patterns of individual features. Explainable Artificial Intelligence (XAI) transforms opaque model behavior into human-intelligible narratives, offering modalities such as Local Explanations, Global Explanations, Rule-based Explanations, and instance-based explanations [28]. Established opaque predictive architectures, while delivering commendable accuracy metrics, habitually obscure the deductive pathways informing their recommendations from the farming community [28]. XAI toolkits, incorporating feature attribution analyses, model internal audits, and counterfactual scenario generation, zero in on these inferential chains, illuminating which determinants within the voluminous agricultural data landscape exert the most pronounced leverage on predictive outcomes [29, 30]. Descriptive labels such as black box, gray box, and white box have gained currency for characterizing gradients of internal accessibility within system components throughout the scholarly literature [31]. At one extreme, a white box element offers total visibility, laying bare every design nuance to the observer. Conversely, gray box components occupy an intermediary position, varying with the extent of disclosed operational specifics. Within the AI

© 2022 The Author(s). | Published by Agro Intelligence Research Press

domain, the black-box predicament denotes the systemic inability to furnish a coherent account of how a particular conclusion was formulated, a phenomenon widely termed "the black-box nature" [32]. This conundrum underscores the barrier to understanding the inner workings of AI systems, hindering stakeholders' ability to trace the logical progression leading to specific determinations. Accordingly, the XAI paradigm plays a pivotal role in mitigating the opacity challenge commonly associated with complex machine learning models [27]. XAI endows machine learning pipelines with both clarity and interoperability. Thus, XAI aspires to lay bare the deliberative sequences of sophisticated machine learning (ML) models, transforming their outputs into artifacts digestible by human cognition. The criticality of XAI intensifies in contexts where algorithmic decisions carry profound ramifications across diverse scholarly disciplines, including medical sciences, agronomy, autonomous navigation systems, and beyond [33]. The foundational imperative of XAI is to cultivate reliance among terminal users. Consequently, AI-synthesized forecasts and adjudications become markedly more approachable and human-centric [34]. This orientation not only engenders accountability and the judicious stewardship of AI technologies but also catalyzes broader adoption by ensuring that end users have the capacity to scrutinize and operationalize AI-derived insights with justified confidence.

Within Sri Lanka's agrarian landscape, cabbage is predominantly categorized as a highland vegetable. Across the 2023 Maha cultivation season, nationwide cabbage harvest volumes attained 52,310.4 metric tons [35]. Although temperate conditions generally favor brassica cultivation, thermotolerant germplasm has been selectively bred to support productive cultivation in arid ecological zones [17, 36]. The Sri Lankan Department of Agriculture prescribes location-specific varietal selections tailored to distinct agroclimatic belts. The Exotic and Hercules cultivars exhibit optimal performance in the up-country wet zone, attributable to their chilling tolerance, whereas Exotic, AS Cross, and KY Cross exhibit superior ecological plasticity in mid-country environments. Attuned to marketplace preferences, plant breeders have synthesized hybrid lines amalgamating commercially desirable attributes, exemplified by offerings under the Royal Sluis, Green Coronet, Golden Cross, Green 123, Tropicana, and GS Cabbage designations [1, 37-39].

The work conducted by Sajindra *et al.* [1] successfully estimated the N, P, and K titers within cabbage production soils utilizing conventional opaque modeling frameworks [1]. That investigation, however, did not interrogate the interpretability dimension of the formulated predictive apparatus. This scholarly endeavor aims to architect an XAI-grounded model to infer soil nitrogen, phosphorus, and potassium status in cabbage cropping systems. By isolating nutrient-specific prognostic tasks, the inquiry aims to enhance model clarity and yield operationally relevant intelligence for precision farming. This methodological orientation directly confronts the deficiencies inherent in classical opaque modeling by unpacking the convoluted associations between cabbage phenotypic expressions and rhizosphere macronutrient reservoirs. The culminating ambition is to empower targeted nutritional intervention protocols that streamline resource use, reduce ecological footprints, and champion enduring agricultural sustainability.

Materials and Methods

Case study data set

Cabbage specimens were propagated systematically in meticulously monitored greenhouse installations, with uncompromising adherence to prescribed benchmarks. The experimental stations consisted of greenhouse facilities positioned in Marassana and Nuwara Eliya, both lying within the Central Province, together with Welimada in Sri Lanka's Uva Province **(Figure 1)**. In each of the aforementioned greenhouse sites, ten Green Coronet cabbage individuals were raised in discrete soil-filled containers expressly for this investigation. The growth regime conformed to uniform environmental parameters and agronomic practices deliberately formulated to foster cabbage maturation, thereby providing a steady, homogeneous cultivation backdrop. These practices spanned the exacting regulation of multiple variables, including ambient temperature, light exposure, moisture content, watering schedules, airflow, and substrate pH, coupled with rigorous enforcement of pest- and disease-management countermeasures [1].

© 2022 The Author(s). | Published by Agro Intelligence Research Press

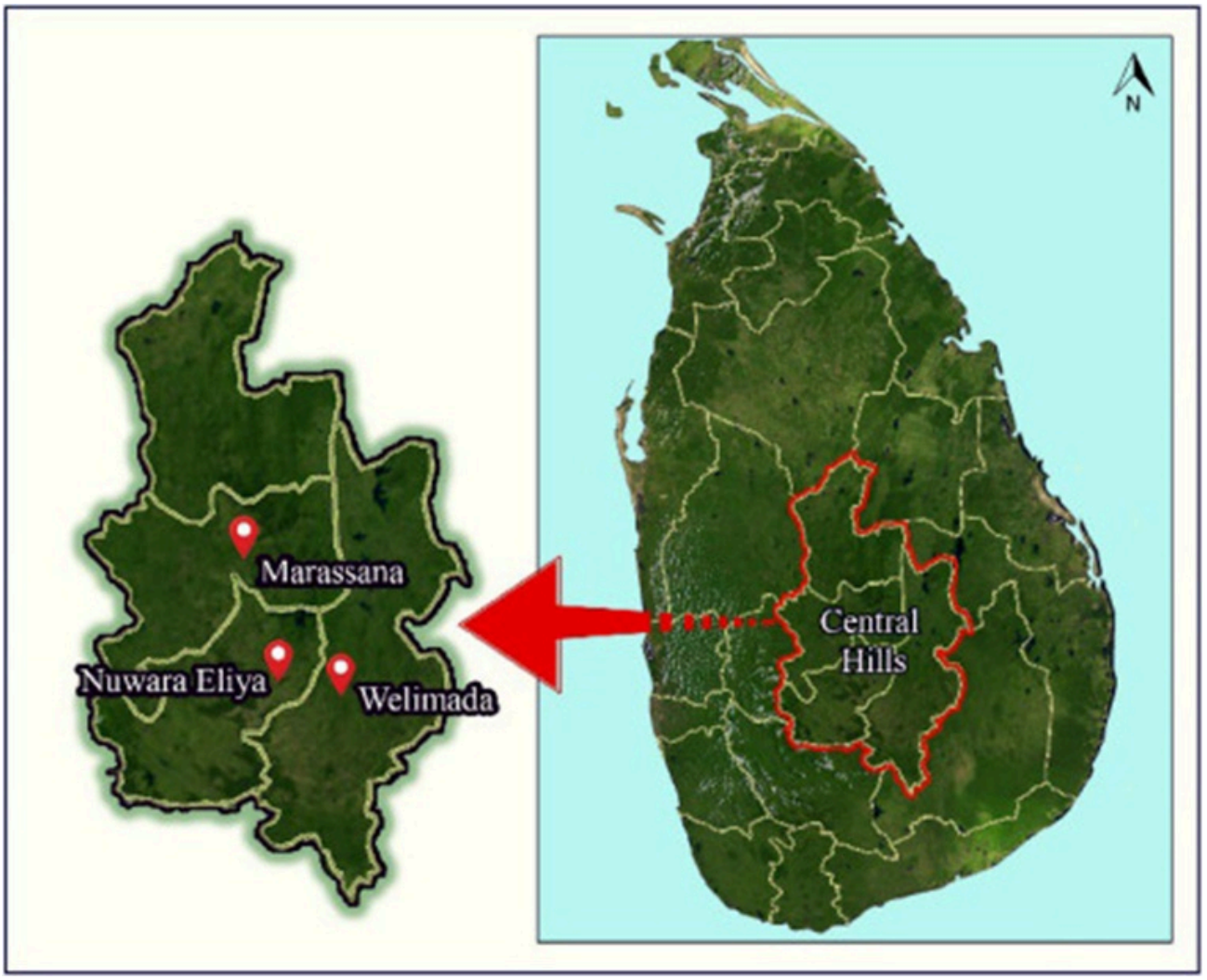

Figure 1. Selected research sites of the central hills in Sri Lanka.

At successive seven-day junctures, the quantities of the three primary soil macronutrients—nitrogen, phosphorus, and potassium—resident within the root-proximate soil zone were assayed by means of an NPK conductivity sensing unit (JXBS3001-DLJ). This tracking regimen spanned the full 85-day window [1].

Macronutrient titers were cataloged in units of milligrams per kilogram (mg kg^{-1}). In parallel, various vegetative growth indicators, namely plant stature, foliage count, and mean leaf expanse, were systematically recorded at 7-day intervals throughout the 85-day surveillance phase. Plant stature, denoted in centimeters (cm), and mean leaf expanse, rendered in square centimeters (cm^2), for each designated individual were established through the use of a supple measuring strip graduated in millimeters (mm) and a portable foliar area quantification device (LI-3000C) [40, 41]. Cabbage plant stature was recorded as the upright span extending from the soil surface to the terminal apex of the specimen at every developmental interval. Foliar surface quantification was performed using an optical scanning head equipped with light-emitting diodes and paired detection elements, enabling accurate area measurement as cabbage foliage traversed the scanning path.

Data set evaluation

The compiled dataset documenting cabbage vegetative progression was entirely free of lacunae, a consequence of the orderly collection of corresponding measurements from both plant subjects and their soil vessels at consistent weekly

© 2022 The Author(s). | Published by Agro Intelligence Research Press

intervals. Additionally, the dataset showed a notable absence of convolution and a rather low standard deviation **(Table 1)**. The dispersion profiles of the respective features are portrayed in **Figure 2**.

Table 1. Descriptive data of factors used in the model.

Days	84	77	70	63	56	49	42	35	28	21	14	7
Mean height	23.37	23.37	23.37	22.13	20.1	19.00	16.27	15.17	10.83	8.1	5.03	0
Mean Average leaf area	382.97	381.73	378.77	354.6	309.37	261.63	192.53	148.63	93.9	53.07	5.57	0
Mean of leaf count	13.60	13.60	13.57	13.5	13.33	11.90	10.33	8.50	5.93	3.73	2.00	0
Mean N content (mg kg-^{1})	19.81	19.99	20.17	21.37	23.82	25.11	30.91	32.47	35.9	40.82	42.27	43.75
Mean P content (mg kg-^{1})	9.43	9.72	10.23	9.83	10.5	10.15	11.27	13.26	14.34	15.63	17.31	19.21
Mean K content (mg kg^{-1})	26.45	26.65	26.41	27.64	28.42	30.45	32.75	38.88	43.01	44.32	45.35	51.55
SD of height	1.14	1.14	1.14	1.23	1.01	1.10	1.00	1.07	0.73	0.75	0.55	0
SD of Average leaf area	27.93	27.72	26.87	35.29	40.54	28.19	13.56	26.76	10.96	7.99	1.15	0
SD of leaf count	0.76	0.76	0.72	0.72	0.75	0.47	0.57	0.56	0.25	0.57	0	0
SD of N content (mg kg^{-1})	0.60	0.63	0.80	0.87	1.15	1.33	1.59	1.67	1.84	1.91	2.01	2.00
SD of P content (mg kg^{-1})	0.64	0.57	0.67	0.57	0.29	0.28	0.37	0.50	0.27	0.49	0.45	0.95
SD of K content (mg kg^{-1})	0.59	0.61	0.63	0.93	0.77	0.84	0.76	1.24	0.82	1.57	1.08	0.73

SD denotes Standard Deviation.

© 2022 The Author(s). | Published by Agro Intelligence Research Press

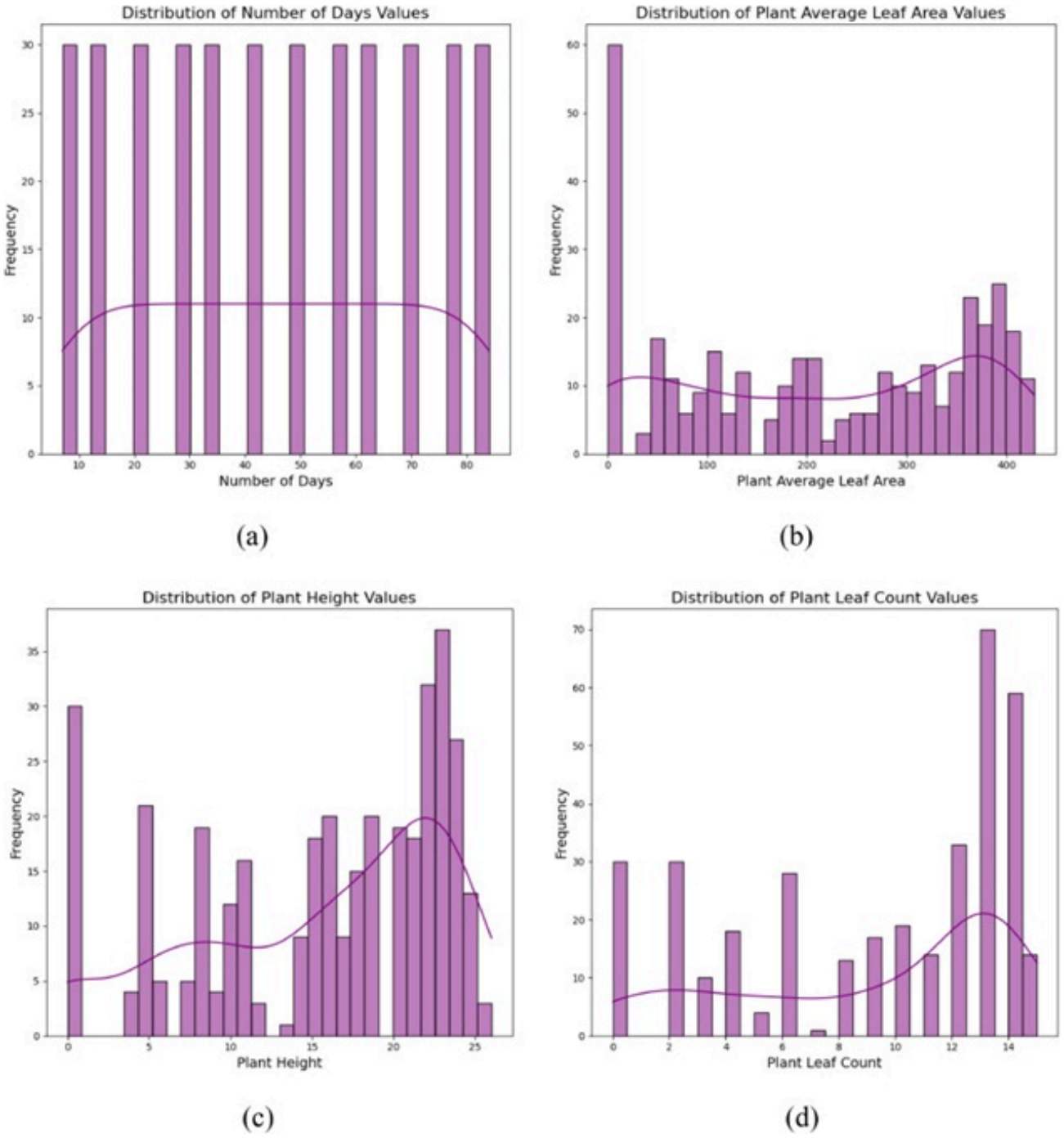

Figure 2. Data distribution of the features (units: Plant Average Leaf Area (cm²); Plant Height (cm)); The components (a), (b), (c), and (d) correspond to the temporal progression in days, mean foliar surface area, plant stature, and foliage number, respectively, with the spread of each attribute scrutinized relative to its occurrence density.

In line with the data spread, the temporal variable (Day) consistently recorded a tally of 30, reflecting the 30 experimental plants tracked across the full 84-day span. The mean foliar surface area, plant stature, and foliage count variables exhibited increasing occurrence frequencies with increasing attribute magnitudes. The spread patterns for the temporal and foliage count variables exhibit relatively sparse value dispersion across the sampling space.

© 2022 The Author(s). | Published by Agro Intelligence Research Press

To provide supplementary elucidation and inform model selection for predictive purposes, an exploratory comparative exercise was conducted among Support Vector Regression (SVR), K-Nearest Neighbors (KNN), Decision Tree, and Artificial Neural Network (ANN) paradigms. Given the comparative outcomes, the ANN architecture was selected to perform the predictive function within the constructed model.

Overview of machine learning models employed in the study

Throughout this inquiry, SVR, KNN, Decision Tree, and ANN computational schemes were marshaled to infer soil nutrient statuses, given their validated track records in analogous agronomic settings. SVR demonstrates particular proficiency in navigating high-dimensional input spaces and disentangling complex variable couplings, making it a suitable candidate for simulating soil nutrient dynamics. KNN offers operational simplicity, coupled with competence in detecting localized structural motifs embedded in the data, a quality that favors soil nutrient inference tasks. Decision Trees provide clear interpretability by delineating branching logic based on feature threshold criteria, thereby helping untangle the differential impact of various determinants on soil nutrient profiles. ANNs are capable of encapsulating highly convoluted, nonlinear correspondences, making them well-suited for detecting subtle patterns woven through soil nutrient repositories. Standardization procedures were applied to the ANN, SVR, and KNN frameworks, using the ‘StandardScaler’ utility. By contrast, for arborescent architectures such as Decision Trees, standardization was deemed superfluous, as these model classes remain agnostic to the absolute magnitudes of input variables; accordingly, they were deployed in their unmodified, unscaled state. By strategically leveraging this heterogeneous ensemble of methodological approaches, the study aimed to isolate models that offer the highest fidelity and greatest interpretability for soil nutrient prognostication, thereby advancing precision agricultural practice.

Support vector regression (SVR)

SVR is a refined, flexible machine learning approach primarily suited to regression-oriented tasks. It constitutes a derivative of the Support Vector Machine, a paradigm classically confined to classification endeavors [42]. The operational principle of SVR is to locate an optimal hyperplane that fits the empirical data while maintaining a permissible deviation zone (epsilon) around the fitted values. This allowance band furnishes the model with a measure of immunity to anomalous data points and stochastic disturbances, rendering SVR especially pertinent to real-world contexts where datasets seldom exhibit ideal cleanliness [43]. A signature capability of SVR is its ability to accommodate nonlinear functional forms via kernel transformations, such as radial basis function, polynomial, and sigmoidal mappings. These kernel operators project the native input coordinates into augmented-dimensional feature embeddings, enabling the model to apprehend intricate structural regularities that purely linear specifications might overlook [44]. That said, SVR imposes stringent requirements on the fine-tuning of its governing hyperparameters—including the regularization weight, the epsilon-insensitive tube radius, and kernel-specific coefficients—to achieve optimal generalization performance [45]. Moreover, despite its robust handling of expansive feature landscapes, SVR can exact a heavy computational toll, particularly when confronted with large data corpora, owing to the need to solve quadratic programming formulations during model fitting [46].

K-Nearest neighbors (KNN)

KNN is among the most elementary yet powerful machine learning formalisms, with broad application across both classification and regression domains [47]. KNN qualifies as a memory-based, distribution-assumption-free inferential scheme, meaning it eschews any presupposition regarding the underlying statistical shape of the data-generating process. Instead, KNN operates by memorizing the entire training corpus and deriving predictions based on the affinity between a newly encountered query point and the archived exemplars [48]. This affinity is typically operationalized through a distance function, with the Euclidean metric being the customary choice, though alternative measures—for instance, Manhattan or Hamming distance—can be used depending on the data typology at hand [49]. The defining operational parameter within KNN is ‘K,’ which specifies the count of proximate neighbors consulted when synthesizing an estimate. Adopting a smaller K renders the estimator acutely responsive to spurious perturbations and isolated irregularities, whereas selecting a larger K yields smoother, more generalized resolution boundaries. Notwithstanding its

© 2022 The Author(s). | Published by Agro Intelligence Research Press

conceptual elegance and ease of implementation, KNN may incur considerable computational overhead during deployment, particularly as dataset volumes swell, because it requires computing pairwise distances for every stored training instance. Furthermore, KNN is highly sensitive to the native scales of predictor variables, making proper data normalization or standardization an indispensable prerequisite for model application [50].

Decision Tree

Decision Trees represent a flexible class of machine learning algorithms suited to both classification and regression problems, valued chiefly for their inherent simplicity and ease of interpretation. The mechanism underlying a Decision Tree involves the recursive subdivision of the feature space into progressively finer partitions, where at each juncture the split is dictated by the most discriminating attribute, identified using metrics such as Gini impurity, information gain, or variance reduction [51]. The resultant architecture expands by spawning internal decision nodes and terminal leaf nodes; each internal branch encodes a conditional test on a particular attribute, while every leaf encapsulates a final predicted outcome [52]. A central merit of Decision Trees is their inherent interpretability—the chain of reasoning that produces a given prediction remains entirely visible, permitting practitioners to trace precisely how conclusions are reached. Conversely, these models exhibit a marked susceptibility to overfitting, particularly in the presence of noisy measurements or highly convoluted data structures, which degrades their capacity to generalize beyond the training corpus. To temper this tendency toward overfitting, pruning procedures are routinely invoked, which strip away superfluous branches that furnish negligible incremental predictive value [53]. Even with these acknowledged drawbacks, Decision Trees readily accommodate both quantitative and categorical predictor types, a characteristic that sustains their widespread utility across numerous application areas [12].

Artificial neural network (ANN)

ANNs constitute a remarkably versatile and potent category of computational models inspired by the organizational principles and signal-processing mechanisms observed in biological nervous systems. ANNs are assembled from layered configurations of interconnected computational units, each unit accepting weighted input signals, applying a nonlinear transformation via an activation function to the aggregated input, and propagating the resulting activation to units in the subsequent layer. The canonical ANN layout typically consists of an input layer, an arbitrary number of hidden layers, and an output layer. It is within these hidden strata that the model progressively distills and encodes the complex, nonlinear mappings that characterize the data-generating process [54]. The training of ANNs proceeds via a methodology known as backpropagation, in which the model systematically adjusts the connection weights between units to drive down the discrepancy between its generated outputs and the observed target values. This weight-tuning process is orchestrated through optimization routines such as gradient descent, which iteratively refines the weight configuration toward a solution that yields minimal predictive error [55]. The extensive adaptability of ANNs has enabled their successful deployment across a broad spectrum of tasks, including visual object identification, automated language understanding, and temporal sequence forecasting [56-58].

Model development and training

A neural network-based computational model was constructed within this study. The design comprises three hidden intermediate processing tiers, excluding the initial receiving layer and the final emitting layer, with each tier hosting 100 computational units. The initial receiving layer has four input nodes, while the terminal emitting layer has three output nodes **(Figure 3)**. The mathematical formulation of the functional relationship approximated in this work is given in **Eq. 1**.

$$\mathbf{N}_{\mathbf{content}}, \mathbf{P}_{\mathbf{content}}, \mathbf{K}_{\mathbf{content}} = \phi \begin{pmatrix} Plant\ Height,\ Number\ of\ Leaves, \\ Average\ Leaf\ Area,\ Number\ of\ Days \end{pmatrix} \quad (1)$$

© 2022 The Author(s). | Published by Agro Intelligence Research Press

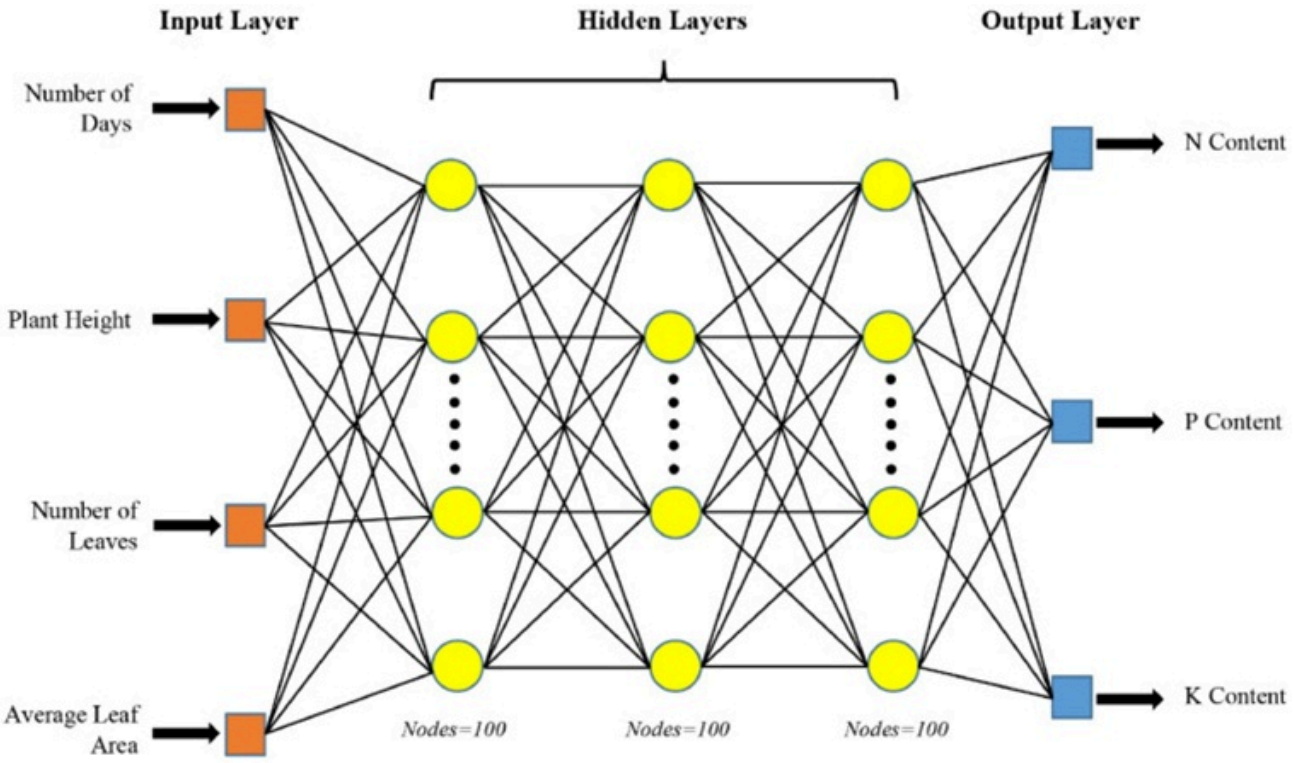

Figure 3. Architecture of the ANN model.

The compiled dataset was partitioned into 80% for model fitting and 20% for independent performance assessment. Beyond this, a separate subset of 15 data points, deliberately chosen to represent all developmental stages of the crop, was extracted for confirmatory validation [59]. In parallel, the SHAP and LIME interpretive frameworks were applied to demystify the model's generated outputs [60]. The SHAP methodology was operationalized to capture the model's overarching, global behavioral tendencies across the entire observational dataset, moving beyond the inspection of any single prediction. Complementarily, the LIME methodology was harnessed to furnish locally faithful, human-comprehensible rationales for the model's individual, case-specific forecasts. The entire analytical pipeline was implemented in Python as the primary programming language. Google Colab served as the cloud-based computational platform, delivering the hardware and software resources essential for both model training and subsequent evaluation [57].

Web Application Architecture and Data Flow

The software instrument was built and deployed in a Google Colab workspace, showcasing an approachable user interface. The bidirectional linkage between the server-side logic and the client-facing display was orchestrated via Ngrok, thereby enabling the estimation of principal soil nutrient stocks from cabbage phenotypic descriptors. Ngrok functions as a versatile API tunneling service, offering immediate, cryptographically secure connectivity for application testing, allowing remote interaction with the locally hosted predictive model without requiring an intricate deployment configuration.

The front-end consists of an HTML-based form incorporating designated entry fields mapped to three salient plant-derived traits, together with weekly temporal increments. Upon the user populating these fields and triggering the submission command, the supplied values are intercepted and relayed via an HTTP POST request to the server-side processing module. At this stage, the previously trained machine learning model, persisted within the cloud storage infrastructure, accepts the incoming feature vector and computes the corresponding nutrient predictions.

Model Integration and Response Handling

© 2022 The Author(s). | Published by Agro Intelligence Research Press

Upon successful receipt of the input payload, the server-side component loads the machine learning model from its .sav file. It injects the incoming data for predictive inference. The model processes the submitted inputs and outputs, forecasting nutrient quantities. These computed estimates are then wrapped within the server's response envelope and transmitted back to the client-facing interface. The HTML document dynamically refreshes to surface the prediction outcomes, furnishing the end user with instantaneous feedback. This entire operational cycle, facilitated by Ngrok, relies on the HTTPS protocol to ensure both the confidentiality and operational efficiency of the communication channel between the client (HTML presentation layer) and the server (model execution environment), all within a cloud-hosted setting.

Performance evaluation

In the present modeling endeavor, 200 training epochs were performed to achieve high precision, yielding 97% accuracy in both the fitting and independent evaluation phases. **Figure 4** depicts the model's learning progression, with the horizontal axis tracking epoch count and the vertical axis recording loss magnitude throughout the fitting stage. The loss metric exhibits a precipitous decline over epochs 0-24 during the fitting phase, as expected. Following this initial descent, the graphical trace shows negligible further variation in the loss value across epochs 75-200. Even so, the model achieved strong accuracy, with only a trivial difference between the training and test accuracies at the 200-epoch ceiling.

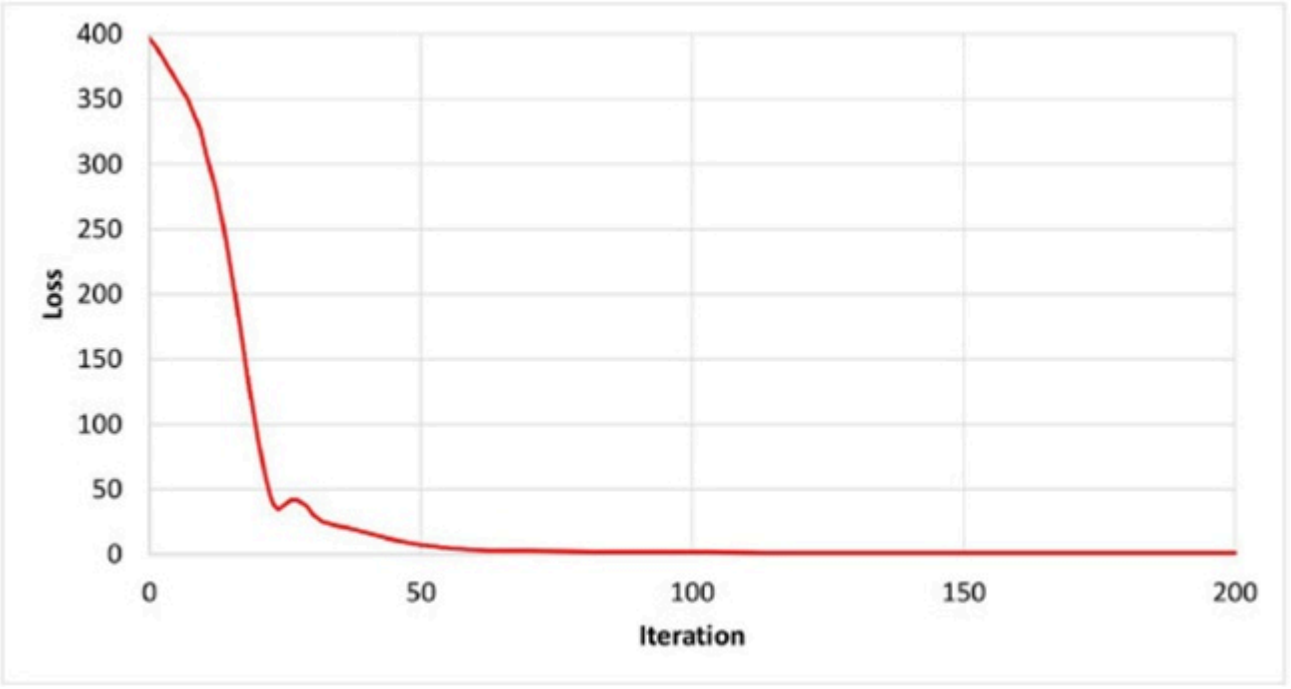

Figure 4. Training stage learning curve of the model.

Once the deep learning model was built, an intuitive, interactive dashboard was engineered. This application was crafted with the express intent of reducing user interaction complexity and amplifying the overall user experience, thereby guaranteeing a fluid, obstacle-free engagement for stakeholders interfacing with the model's functional repertoire.

Shapley additive explanations (SHAP)

The SHAP interpretive paradigm seeks to render a model's predictive outputs intelligible by apportioning credit—quantified as marginal contributions—across the suite of input features [61]. To accomplish this, it adapts the Shapley Value construct, originally conceived within the domain of cooperative game theory. By extension, SHAP inherits the axiomatic underpinnings of coalitional game theory when assigning importance scores to individual features. Beyond this,

© 2022 The Author(s). | Published by Agro Intelligence Research Press

SHAP can deliver both localized, instance-level and holistic, dataset-level perspectives on the behavioral characteristics of a machine learning model [62-64]. Lundberg and Lee [61] championed the use of the Shapley value calculus to derive feature attribution metrics. In complementary scholarship, Liang *et al.* [65] outlined an elaborate classification scheme for explanation modalities, positioning SHAP squarely within the category of data-grounded, perturbation-reliant techniques.

As a consequence, SHAP's operation depends on the supplied input variables and does not require familiarity with the target machine learning model's internal computational mechanics [62, 63]. Lundberg and Lee [61] also introduced a family of SHAP implementations optimized for specific model archetypes, including DeepSHAP, Kernel SHAP, LinearSHAP, and TreeSHAP [66]. Within the scope of this investigation, Kernel SHAP was selected as the instrument to shed light on the deep learning model's predictive reasoning. Furthermore, the present research effort draws upon the Keras, Scikit-learn (Sklearn), Matplotlib, NumPy, Pandas, and SHAP programmatic libraries for its technical realization.

Lundberg and Lee [61] established that by casting a weighted linear regression model as a local surrogate—and coupling it with a purpose-designed weighting kernel—the resulting regression coefficients of the LIME surrogate serve directly as estimators of the target SHAP values. The specific Shapley weighting kernel used to derive SHAP values is detailed below **(Eq. 2)**.

$$\pi_{x'}\left(z'\right) = \frac{(M-1)}{(M\ chose|z'|)|z'|(M-|z'|)} \quad (2)$$

Here, M designates the dimensionality of the feature space, whereas |z′| captures the count of features assuming non-zero values within the simplified binary input representation z′. The centrality of Shapley values within the broader XAI enterprise can be articulated through the unifying lens of additive feature attribution methodologies [67]. At its conceptual core, SHAP measures the incremental contribution of each distinct feature (player) to the final model prediction (game).

Local interpretable model agnostic explanations (LIME)

LIME represents yet another post-hoc interpretability instrument within the XAI repertoire, tailored specifically to localized, instance-level elucidation. The LIME paradigm is purpose-built to provide credible explanations for the outputs of arbitrary classifiers or regressors. It does so by constructing a locally faithful surrogate—an intrinsically interpretable model—within the neighborhood of interest for prediction. The method places a premium on yielding explanations that strike a balance between conceptual simplicity and stringent local reliability. Local reliability, in this context, mandates that the explanation rendered for a particular forecast accurately mirrors the original model's response characteristics within a tightly circumscribed region enveloping that forecast instance [68]. LIME follows a regimented sequence to unpack model predictions. The workflow commences by generating a synthetic sample ensemble near the instance awaiting explanation, after which the original model is queried to produce predictions for these newly generated samples. Each perturbed sample is subsequently assigned a weight reflecting its similarity or proximity to the focal instance. This disciplined procedural pipeline enables LIME to deliver both dependable and human-intelligible rationales for single-instance predictions, thereby contributing materially to the transparency and cognitive accessibility of sophisticated ML constructs [69].

Harnessing the class probability scores or continuous output values harvested from the collection of samples populating the relevant input neighborhood, LIME proceeds to fit a sparse linear surrogate. The fitted coefficients of this simplified proxy then serve as quantitative indicators of the relevance of individual input covariates. A further virtue lies in LIME's agnostic posture toward the underlying model class, which ensures broad-spectrum applicability across heterogeneous machine learning formalisms without functional constraints [68, 69].

Overall methodology

© 2022 The Author(s). | Published by Agro Intelligence Research Press

To convey a fully integrated view of the procedural workflow, the holistic methodological sequence is rendered as a block diagram in **Figure 5**. The enumerated actions listed below were carried out:

1. The web-based tool is initialized inside the cloud-hosted workspace.

2. A secure tunneling conduit is established to the private cloud workspace via a designated port by invoking the ‘Ngrok’ executable.

3. The ephemeral, publicly routable URL is broadcast.

4. The allocated URL is circulated to the intended end users who will interact with the web-based tool.

5. End-users navigate to the supplied web address through standard internet access.

6. As the inbound request arrives at the ‘Ngrok’ web server (since the URL is anchored to an ngrok.com subdomain, all incoming traffic is initially directed toward the ‘Ngrok’ web server), the server undertakes a routing operation, resolving the URL to the specific application earmarked for tunneling.

7. Ngrok subsequently relays the request over the encrypted tunnel created in Step 2.

8. The forwarded request is patched through and establishes a session with the target application.

© 2022 The Author(s). | Published by Agro Intelligence Research Press

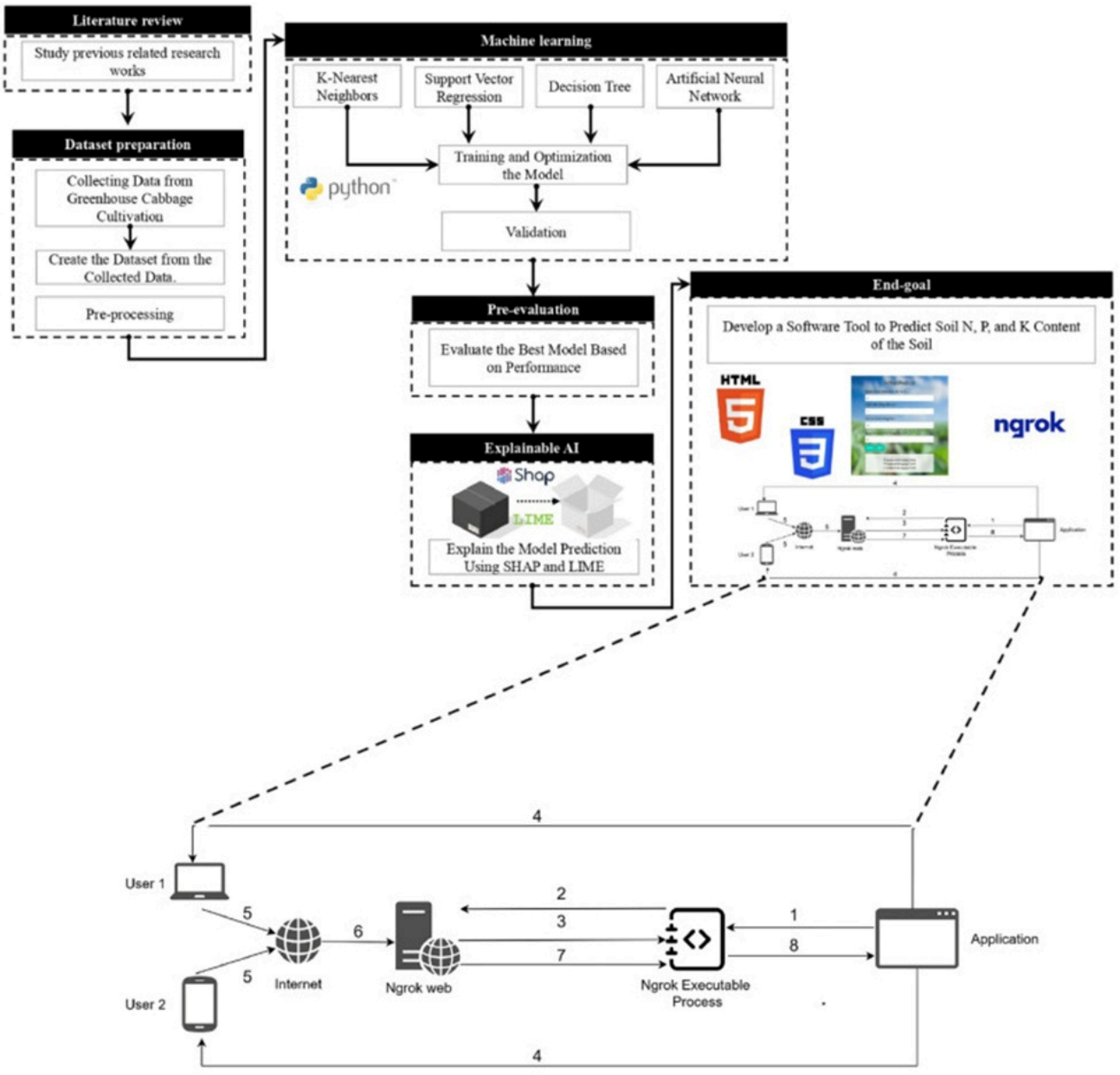

Figure 5. Flow diagram of the study.

Model accuracy evaluation

The coefficient of determination, customarily notated as R^2, is a statistical yardstick that captures the proportion of total variance residing in the dependent variable (y) that is collectively accounted for by the independent variable(s) (x) within a regression construct. Rephrased: it calibrates the congruence between the model's fitted curve and the empirically observed data. The defining expression for R^2 is furnished in **Eq. 3**.

$$R^2 = 1 - \frac{\sum (y_i - \hat{y}_i)^2}{\sum (y_i - \bar{y})^2} \quad (3)$$

© 2022 The Author(s). | Published by Agro Intelligence Research Press

In this notation, yi corresponds to the genuine observed y readings, while yiˆ stands for the model-projected y values. The symbol $\bar{y}$ denotes the arithmetic average computed over the y observations. SSR, the regression sum of squares, is a statistical construct employed to encapsulate the quantum of variation in the response variable (y) that finds explanation through the independent variable(s) (x) in a regression setting. Put succinctly, SSR evaluates how closely the regression line fits the empirical data scatter. SST, the total sum of squares, is a descriptive statistic embodying the aggregate variability manifest in the response variable (y), computed without invoking any explanatory covariate. It captures the scatter of the observed y values around their collective mean (ȳ), abstracted away from any dependency on the independent variable(s) [70].

The mean squared error (MSE) is a statistical index that computes the expected value of the squared residuals—the discrepancies between observed and model-forecasted outcomes. In regression diagnostics, MSE is commonly used to gauge the precision of a predictive model **(Eq. 4)** [1].

$$\mathrm{MSE} = \frac{\sum_{i=1}^{N}[x_i - y_i]}{N} \quad (4)$$

Permit x to represent the empirically recorded measurements and y to designate the predicted extremal value ascribed to a given data instance, indexed sequentially from i through n. The scalar N signifies the aggregate number of observations under consideration.

MBE **(Eq. 5)**, an initialism for Mean Bias Error, describes a diagnostic statistic mobilized to scrutinize the accuracy of a predictive model by computing the arithmetic mean of the systematic offset between forecasted and observed quantities. This metric helps determine whether a model harbors a persistent tendency to systematically over- or underpredict the actual magnitudes. A positively signed MBE communicates that the model, on average, overshoots the observed readings, whereas a negatively signed MBE conveys that the model, on average, undershoots them. This evaluative instrument proves especially instructive for benchmarking model fidelity and for diagnosing the directional character of embedded bias.

$$\mathrm{MBE} = \frac{1}{n}\sum_{i=n}^{n}(P_i - O_i) \quad (5)$$

Here, n denotes the complete enumeration of observations or data entries, Pi corresponds to the model-forecasted quantity for the i-th data record, and Oi denotes the empirically observed (actual) quantity for that same i-th data record.

Results and Discussion

Pre-evaluation and model predictions

The findings arising from the preliminary comparative screening of the SVR, KNN, Decision Tree, and ANN frameworks are tabulated in **Table 2**. This portion elaborates on the functional role assumed by predictor variables—specifically, mean leaf surface area, plant stature, leaf enumeration, and chronological progression in days—within each candidate modeling framework, while simultaneously reporting the associated performance diagnostics—namely R^2, RMSE, MSE, and MBE—collated across the evaluated model set.

Table 2. Descriptive data of factors used in the model.

Index	Testing				Training			

© 2022 The Author(s). | Published by Agro Intelligence Research Press

Empty Cell	ANN	Decision Tree	KNN	SVR	ANN	Decision Tree	KNN	SVR
R^2	**0.97**	0.85	0.69	0.87	**0.96**	0.79	0.70	0.86
RMSE	**1.09**	2.97	4.14	3.03	**1.35**	3.15	3.83	2.89
MSE	**1.18**	8.80	17.15	9.19	**1.82**	9.90	14.69	8.37
MBE	−0.01	0.05	−1.53	−0.89	0.11	−0.13	−1.13	−0.67

Drawing inferences from the empirical results, comparatively subdued R^2 statistics of 0.70 and 0.69 for the fitting and testing partitions, respectively, were returned by the KNN formulation, whereas the ceiling R^2 values were documented for the ANN construct, attaining 0.96 and 0.97 for fitting and testing, respectively. This pattern indicates that the ANN configuration achieved markedly stronger regression performance than any of the rival architectures. Extending this analysis, the recorded data confirm that KNN produced the largest MSE and RMSE, with values of 14.69 and 3.83 in the fitting phase, and 17.15 and 4.14 in the testing phase. At the opposite end of the spectrum, ANN produced the most compressed MSE and RMSE figures, recorded as 1.82 and 1.35 during fitting, and 1.18 and 1.09 during testing. These empirical trends collectively indicate that ANN is the most faithful modeling option, outstripping its competitors in both point-prediction precision and the suppression of residual error magnitudes. To lend additional evidential weight to the comparative model assessment, **Figure 6** juxtaposes observed and predicted values through scatter diagrams for both the fitting and testing subsets for each candidate model. The ANN variant exhibits the most exemplary behavioral profile, with only trivial excursions beyond the ±10% and ±20% error envelope boundaries, while simultaneously achieving elevated R^2 coefficients for both fitting and testing **(Figures 6d and 6h)**. Across both graphical presentations, the complete set of observed-versus-predicted coordinate pairs crowds tightly around the identity regression diagonal, testifying to the model's restrained error.

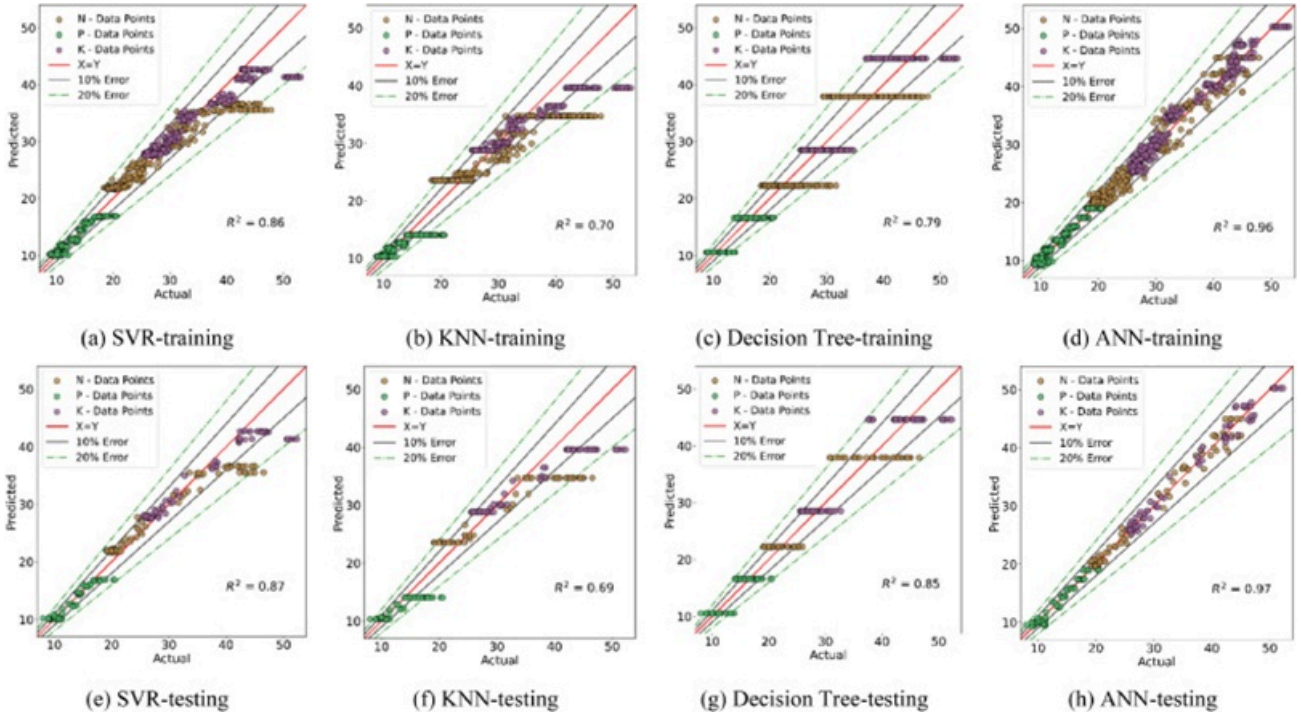

Figure 6. Comparison of actual and predicted values with different Models: Subfigures (a) through (d) map onto the fitting outcomes of the respective models, whereas subfigures (e) through (h) map onto their testing outcomes.

© 2022 The Author(s). | Published by Agro Intelligence Research Press

When examining the MBE metrics, the ANN architecture yielded the closest fitting and testing values to the neutral null benchmark, with computed values of 0.11 and −0.01, respectively. This configuration implies that the model exhibits only marginal tendencies toward either systematic overprediction or systematic underprediction in both the fitting and testing regimes, thereby signaling attenuated systematic bias and sound predictive calibration relative to the competing model cohort. Synthesizing the full spectrum of comparative diagnostics—R^2, RMSE, MSE, and MBE—the ANN modeling paradigm emerges as the unequivocally superior overall performer.

Explanation of model predictions using SHAP

Figure 7 visualizes the differential contributions of each input feature to the estimation of soil N, P, and K stocks.

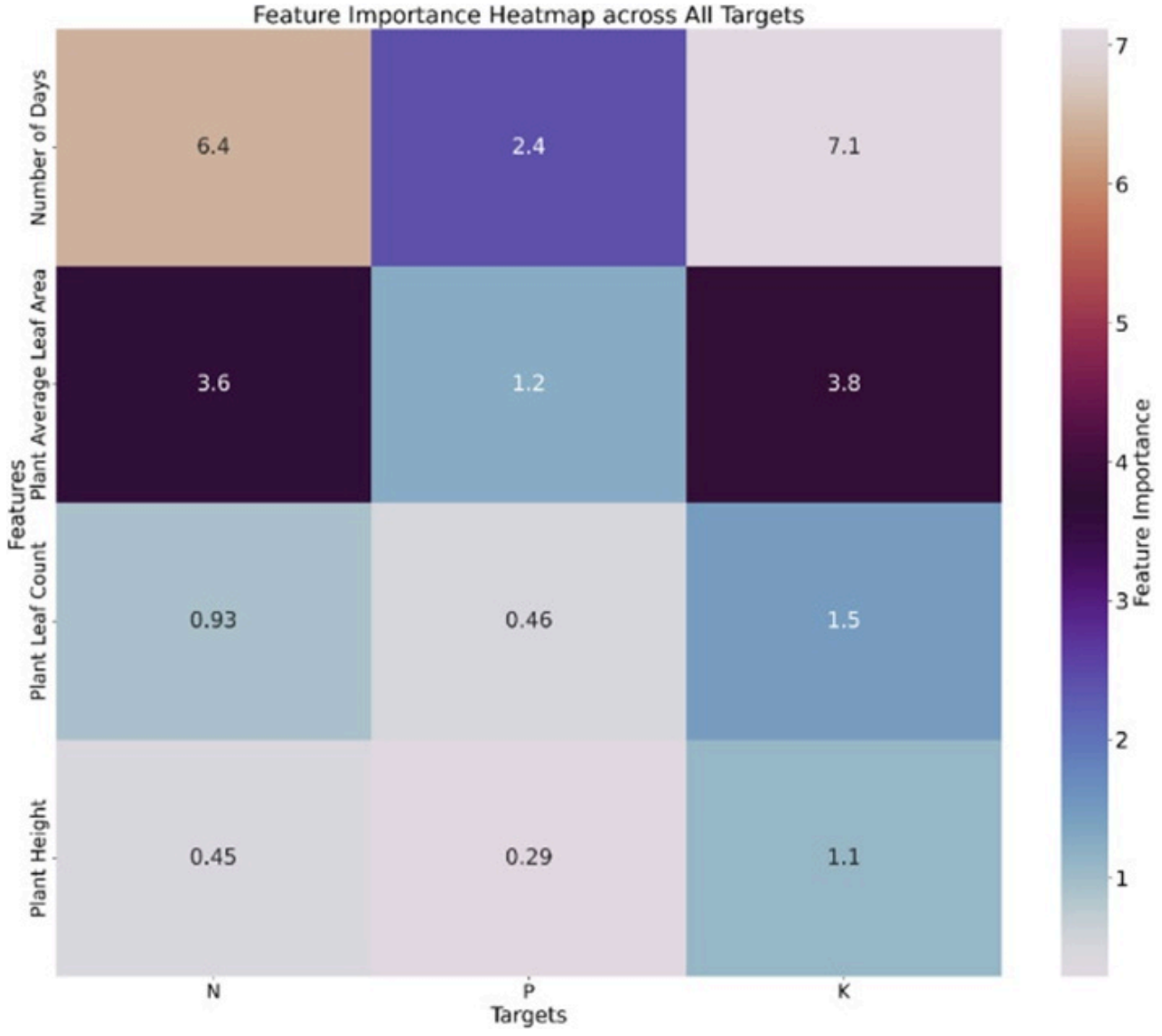

Figure 7. Each feature's importance for the prediction.

In the heatmap rendering, the chromatic scale encodes the magnitudes of numerical contributions, capturing the relative influence of disparate features on the prediction of N, P, and K levels. Features registering elevated numerical intensities within the heatmap carry commensurately greater weight in shaping the respective nutrient forecasts. Consistent with the evidence presented in **Figure 7**, the Day variable exerted the greatest leverage on predicting both soil N and K. In

© 2022 The Author(s). | Published by Agro Intelligence Research Press

contrast, the Plant Height variable consistently exerted the weakest influence across the predictive targets. The weakest overall impact on model forecasts was traced to the prediction of soil N content via the Plant Height variable. In contrast, the strongest overall impact was traced to the prediction of soil K content via the Day variable.

Figure 8 offers a dataset-spanning, globally aggregated representation, wherein SHAP values are spread along the abscissa, encoding both the polarity and the magnitude of their effect on the model's response. The ordinate catalogs the features incorporated within the model. As the underlying feature values transition from low to high, the associated color palette shifts from blue to red, providing a visual shorthand for the shift in feature magnitude [71].

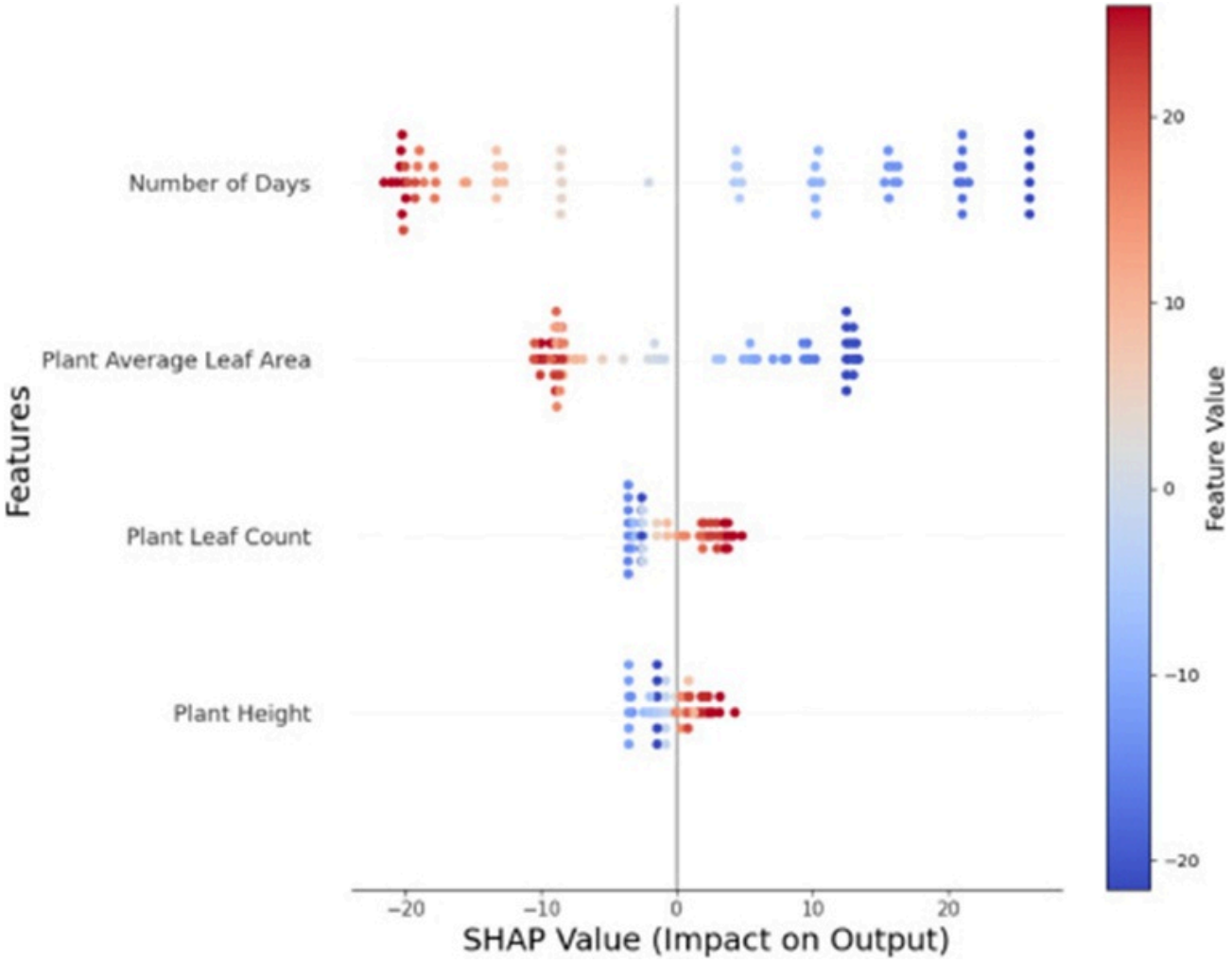

Figure 8. SHAP values for the different features used in the model.

The residual titers of soil N, P, and K bear significantly upon an array of plant traits: stature, foliar count, mean leaf surface area, and elapsed days. This bearing is inferred from the spread and positioning of feature magnitudes relative to their corresponding SHAP scores. Probing SHAP signatures yields instructive insights into the dynamic interdependencies that bind diverse determinants to the model's predictive fidelity. To begin with, upward movement in the elapsed days feature suppresses the model's nutrient content projections, as evidenced by the predominance of negatively signed SHAP scores. Following a similar pattern, as the mean leaf surface area feature increases, the model's soil nutrient forecasts exhibit an adverse perturbation, reflected in the accumulation of negative SHAP scores.

By marked contrast, a rise in the foliar count feature improves the model's soil nutrient forecasts, as evidenced by positively signed SHAP scores. In a congruent manner, increases in plant stature features are associated with more

© 2022 The Author(s). | Published by Agro Intelligence Research Press

precise nutrient predictions, as evidenced by the emergence of positive SHAP scores. This empirical pattern suggests that as both leaf enumeration and plant height progress over the course of the growth cycle, the model draws on increasingly resilient and more discriminative feature signatures, thereby honing its capacity to deliver reliable prognostications. When interpreted holistically, these revelations bring into sharp relief the convoluted interplay connecting temporal variables—such as cultivation cycle duration and the continuously transforming morphological profile of the plant—with their downstream ramifications for the model's predictive capability, reinforcing the imperative of accommodating these dynamic feedbacks within the architecture of agricultural modeling and interpretive analytics.

Explanation of model predictions using LIME

To interrogate the model's behavior at the level of individual forecasts, LIME was applied to six purposefully selected data points [72], arranged in matched pairs across three intensity bands—termed high, medium, and low. These selections mapped onto distinct moments along the crop's developmental trajectory: the concluding phase nearing commercial maturity, the intermediate vegetative bulking stage, and the earliest phase following field establishment.

Inspection of the first high-band case revealed that the covariates Plant Height and Plant Leaf Count exerted facilitatory effects on the estimation of N, P, and K, with positive influence quotients of 1.3, 0.68, 1.92, and 2.45, 1.22, 3.78, respectively, thereby elevating the predicted nutrient readings. Running counter to this trend, the covariates Average Leaf Area and Day functioned as suppressors of the N, P, and K estimates, with negative influence quotients respectively registering −5.84, −1.88, −6.05, and −10.21, −3.52, −10.80, thereby dragging the forecasts downward. Turning to the companion high-band case, Plant Height and Plant Leaf Count upheld their role as elevators of the N, P, and K projections, posting values of 1.25, 0.74, 1.65, and 1.20, 0.43, 1.57. In opposition, Average Leaf Area and Day maintained their suppressive character, returning −5.84, −1.88, −6.05, and −10.21, −3.52, −10.80 for the three macronutrients.

Pulling together the evidence from the dual high-band instances, as rendered in **Figures 9a–9c and 9d–9f**, a coherent narrative takes shape: the projected soil K status receives upward pressure from foliar abundance and plant stature, yet is subject to downward pressure from chronological progression and mean foliar dimensions. This dualistic pattern extends faithfully to soil N prognostication, where foliar count and stature act as amplifiers, while day accumulation and mean leaf area act as dampeners. The same structural dynamic governs soil P inference: stature and foliar abundance enhance estimates, whereas elapsed time and foliar spread diminish them. Collectively, these patterns suggest that certain above-ground expressions—heightened leaf production and vertical elongation—provide the model with signals that aid nutrient inference, whereas advancing days and expanding individual leaf size systematically confound its estimates. The single strongest suppressive force across both high-band examples was wielded by the Day variable (−10.80). In contrast, the strongest promoting force (3.78) originated from the leaf count variable, observed in the first high-band instance during soil K estimation **(Figure 9c)**. In the second high-band example, the dominant promoting signal (1.65) emanated from Plant Height, likewise for soil K.

© 2022 The Author(s). | Published by Agro Intelligence Research Press

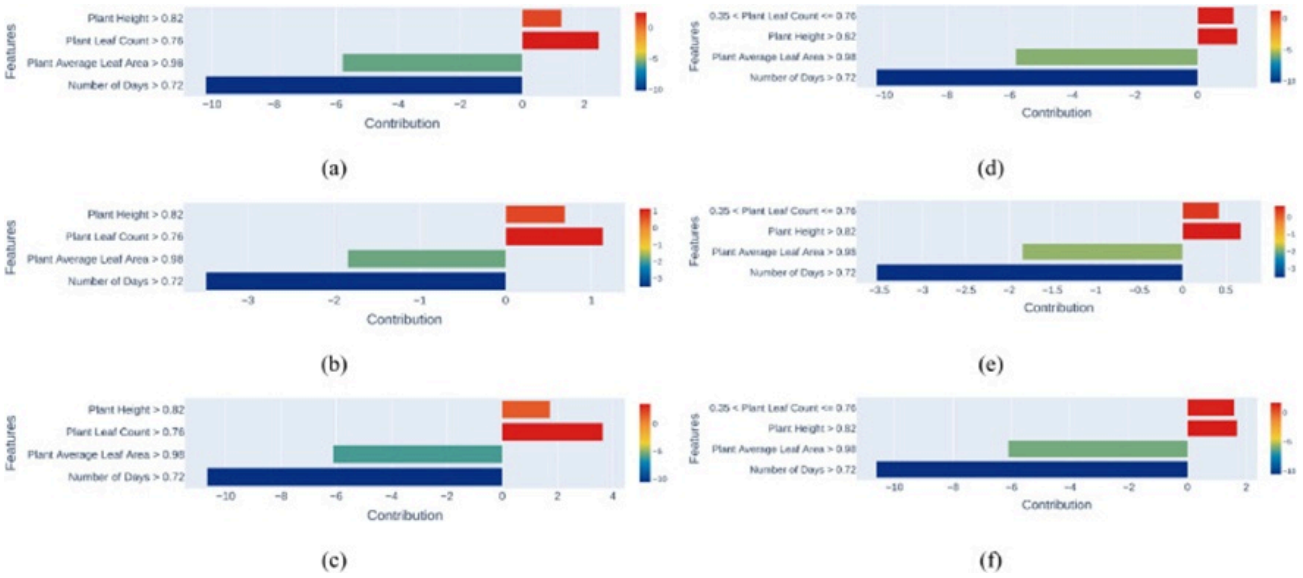

Figure 9. LIME graphs for selected two high instances: (a), (b), and (c) represent the contribution of features for predicting soil N, P, and K, respectively, in the 1st high instance; (d), (e), and (f) represent the contribution of features for predicting soil N, P, and K, respectively, in the 2nd high instance of the testing data.

Progressing to the first medium-band case, the variable Average Leaf Area emerged as a net promoter of the N, P, and K forecasts, with influence scores of 1.5, 0.4, and 1.69, respectively. In contradistinction, the triplet comprising Day, Plant Leaf Count, and Plant Height uniformly exerted depressive effects on the three nutrient predictions, logging −0.1, −0.17, −0.08; −1.22, −0.52, −1.78; and −1.27, −0.71, −1.72 respectively. The second medium-band instance presented a mirror-image configuration: Plant Leaf Count registered as a promoter of N, P, and K forecasts, with attributions of 1.04, 1.03, and 1.94, whereas Day, Plant Height, and Average Leaf Area collectively registered as suppressors, delivering −0.32, −0.35, −0.30; −1.34, −0.73, −1.81; and −4.21, −1.57, −5.10, respectively.

Drawing broader inferences from the pair of medium-band exemplars discloses an intriguing polarity shift. For soil N estimation, the Average Leaf Area variable confers a promotional impetus in the first instance **(Figure 10a)** yet pivots to a depressant role in the second **(Figure 10d)**. Reciprocally, Plant Leaf Count serves as a depressant in the first **(Figure 10a)** and transitions to a promotor in the second **(Figure 10d)**. Both Day and Plant Height, irrespective of the case examined, act as unwavering inhibitors of soil K estimation. This identical flip-flop dynamic replays itself in the context of soil P estimation: Average Leaf Area uplifts predictions in the first medium-band sample **(Figure 10b)** and lowers them in the second **(Figure 10e)**. In comparison, Plant Leaf Count does the reverse—lowering in the first **(Figure 10b)** and uplifting in the second **(Figure 10e)**. Day and Plant Height remain steadfast negative contributors. This symmetrical duality carries forward undiluted to soil K forecasting: Average Leaf Area acts as a positive contributor in the first example **(Figure 10c)** and a negative one in the second **(Figure 10f)**, whereas Plant Leaf Count suppresses in the first **(Figure 10c)** and amplifies in the second **(Figure 10f)**, with Day and Plant Height perpetually aligned as negative contributors. The extreme bounds of influence in the first medium-band sample peaked at +1.69 and −1.78, while the second medium-band sample spanned +1.94 to −5.10, each pair associated with soil K estimation.

© 2022 The Author(s). | Published by Agro Intelligence Research Press

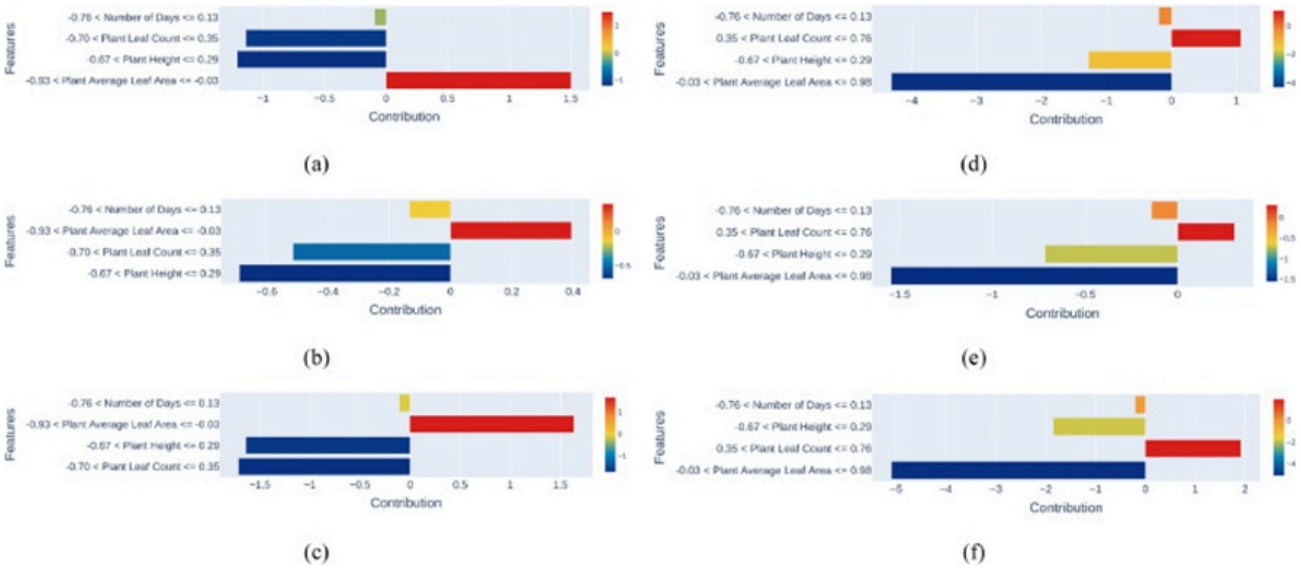

Figure 10. LIME graphs for selected two medium instances: (a), (b), and (c) represent the contribution of features for predicting soil N, P, and K, respectively, in the 1st medium instance; (d), (e), and (f) represent the contribution of features for predicting soil N, P, and K, respectively, in the 2nd medium instance of the testing data.

Turning attention to the low-band segment, the first exemplar shows that Average Leaf Area and Day variables jointly propelled the N, P, and K predictions upward, with substantial influence magnitudes of 9.07, 3.24, 9.16, and 13, 4.1, 13.72, respectively, qualifying them as the dominant positive drivers. A nearly imperceptible upward nudge for soil N estimation was attributed to Plant Height, with a value of merely 0.01. On the opposing flank, Plant Height and Plant Leaf Count weighed negatively on P and K predictions, producing −0.20, −0.30, and −0.91, −3.96, while Plant Leaf Count additionally depressed the N prediction with a score of −2.45. The second low-band exemplar largely reproduced this directional architecture: Average Leaf Area and Day sustained their promotional influence on N, P, and K forecasts, generating 1.45, 0.48, 1.76, and 13.11, 4.66, 13.71. Once more, Plant Height provided a small positive boost to N estimation (0.08). Meanwhile, Plant Height and Plant Leaf Count depressed P and K estimates, yielding −0.03, −0.50, and −0.93, −3.77, with Plant Leaf Count also exerting a negative drag on N estimation (−2.70).

When distilling the joint behavior across the two low-band exemplars for soil N prognosis, the variables Average Leaf Area, Plant Height, and Day uniformly align as constructive forces—all bearing positive influence signs—whereas Plant Leaf Count emerges as the solitary destructive force, consistently bearing a negative sign **(Figures 11a and 11d)**. For soil P prognosis within the same low-band dyad, Average Leaf Area and Day persist as constructive contributors, while the duo of Plant Leaf Count and Plant Height act as destructive ones **(Figure 11)**. An isomorphic attribution structure governs soil K prognosis: Average Leaf Area and Day sustain their constructive orientation. At the same time, Plant Leaf Count and Plant Height maintain their destructive orientation **(Figure 11)**. The outermost positive and negative influence values recorded in the first low-band instance reached 13.72 and −3.96, respectively; in the second instance, the corresponding extremes were 13.7 and -3.77, each set connected to the estimation of soil K reserves.

© 2022 The Author(s). | Published by Agro Intelligence Research Press

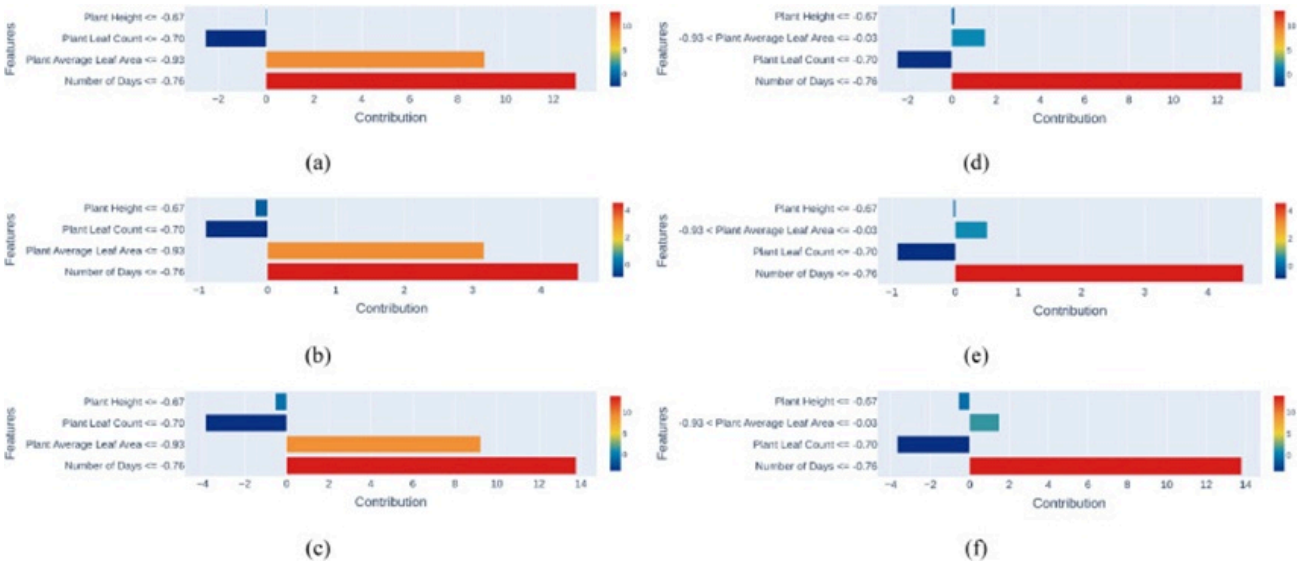

Figure 11. LIME graphs for selected two low instances: (a), (b), and (c) represent the contribution of features for predicting soil N, P, and K, respectively, in the 1st low instance; (d), (e), and (f) represent the contribution of features for predicting soil N, P, and K, respectively, in the 2nd low instance of the testing data.

‘SoilNutriPredictor’ web application

Drawing on the experimental outcomes, a web-based computational instrument, designated "SoilNutriPredictor," was constructed, incorporating an interface deliberately crafted for ease of operation **(Figure 12)** to minimize the technical burden on its intended operators. The system accepts four user-supplied arguments: the count of weeks elapsed since planting, the vertical extent of the cabbage specimen in centimeters, the total enumeration of foliage units borne by the plant, and the arithmetic mean of individual leaf lamina spread expressed in square centimeters. These raw entries are first routed through a feature standardization pipeline before being presented to the trained deep neural architecture. Based solely on these above-ground morphological descriptors, the model infers rhizosphere concentrations of N, P, and K and reports its estimates in the conventional units of milligrams per kilogram (mg kg^{-1}). Additionally, the interface incorporates a dedicated reset control that instantly purges all previously entered fields and restores the form to its pristine state, readying it for a subsequent prediction cycle.

© 2022 The Author(s). | Published by Agro Intelligence Research Press

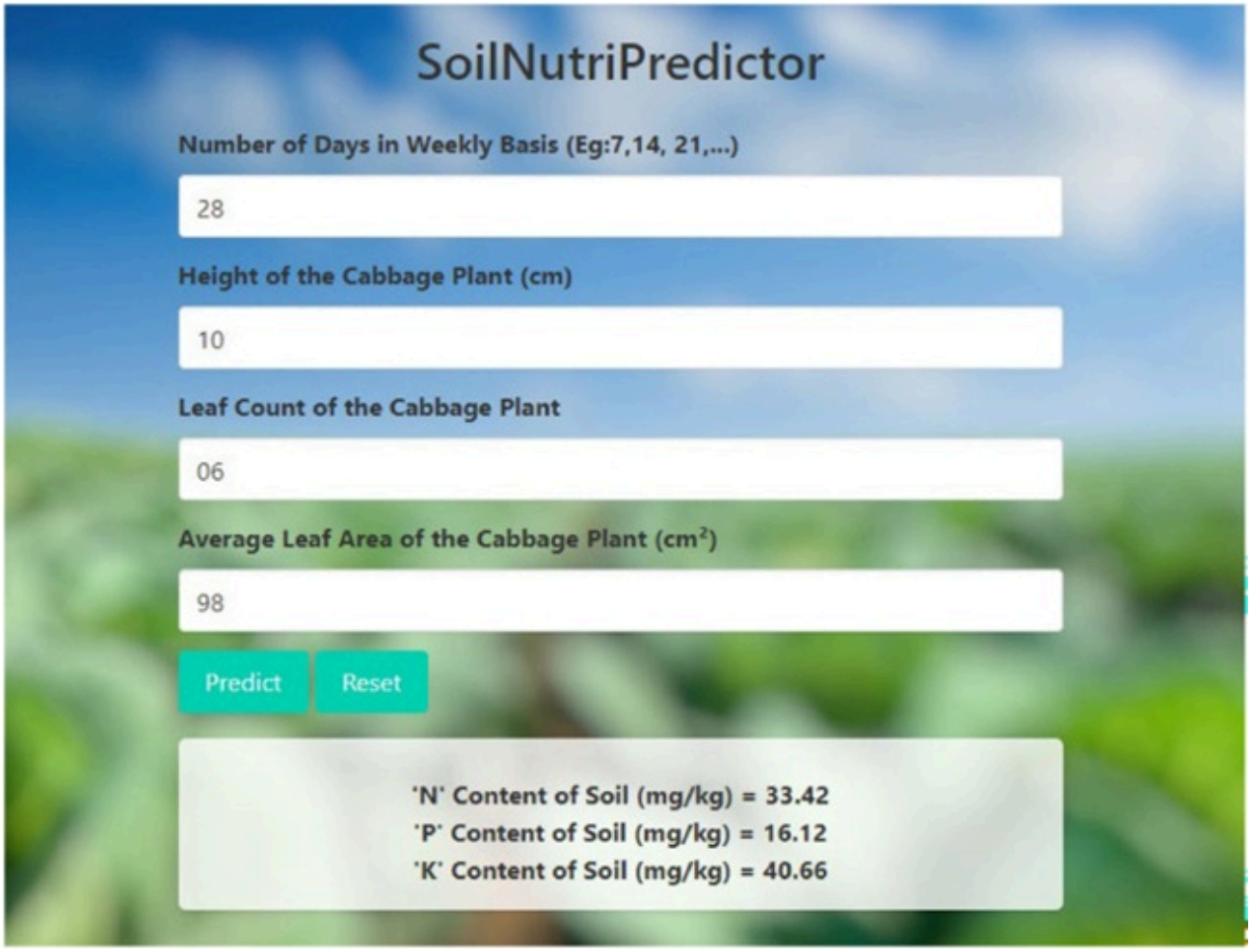

Figure 12. 'SoilNutriPredictor' web application interface.

The delivery of an intuitive software instrument that can be operated directly by agricultural practitioners constitutes a noteworthy contribution in its own right. This development dovetails with and actively promotes the overarching philosophy of food system resilience and agrarian sustainability, thereby advancing the aspirations codified under Sustainable Development Goal 2—"Zero Hunger." Questions surrounding the long-term viability of food production networks command intense interest across numerous societal strata, particularly in an era marked by rapid demographic growth. Accordingly, the methodological and technological progress reported in the present study has considerable practical relevance for determining fertilization rates that strike an optimal balance, enabling cultivators to achieve peak productive returns. A further ancillary benefit conferred by the modeling framework concerns the attenuation of nutrient export via surficial water movement. By guiding more judicious application rates, the tool indirectly helps mitigate eutrophication in receiving water bodies adjacent to cultivated parcels.

Software applications designed for portable handheld devices have achieved widespread adoption among contemporary populations—agricultural communities included—a phenomenon driven by their inherent user-friendliness and the relentless advancement of smartphone technology. This reality provides a strong rationale for porting the current browser-based tool to a dedicated mobile format. Looking ahead, subsequent investigative phases could aim to automate the acquisition of all required predictor measurements—specifically, temporal stage, stature, leaf enumeration, and mean leaf surface area—by deploying computer vision algorithms. Attaining such a capability would empower growers and field extension personnel to retrieve predicted soil nutrient status virtually instantaneously and directly in the field, eliminating

© 2022 The Author(s). | Published by Agro Intelligence Research Press

the need for time-intensive manual data collection. Such a trajectory points unmistakably toward the maturation of Internet of Things (IoT) ecosystems within the agricultural sphere.

Verification of the predictive apparatus was accomplished through trials involving freshly cultivated, randomly chosen greenhouse cabbage individuals representing a spectrum of phenological progress. A dedicated validation partition comprising 15 contemporaneously acquired observational data records was reserved expressly for this confirmatory exercise. Following the generation of model-based estimates, a comparative analysis was performed between these inferred values and the empirically determined ground-truth measurements, with the resulting deviations depicted graphically **(Figure 13)**. The forecast outputs exhibited only marginal divergences from the corresponding real-time field observations, thereby furnishing compelling evidence that the model executes its predictive function with a high degree of exactitude and acceptably low residual discrepancies.

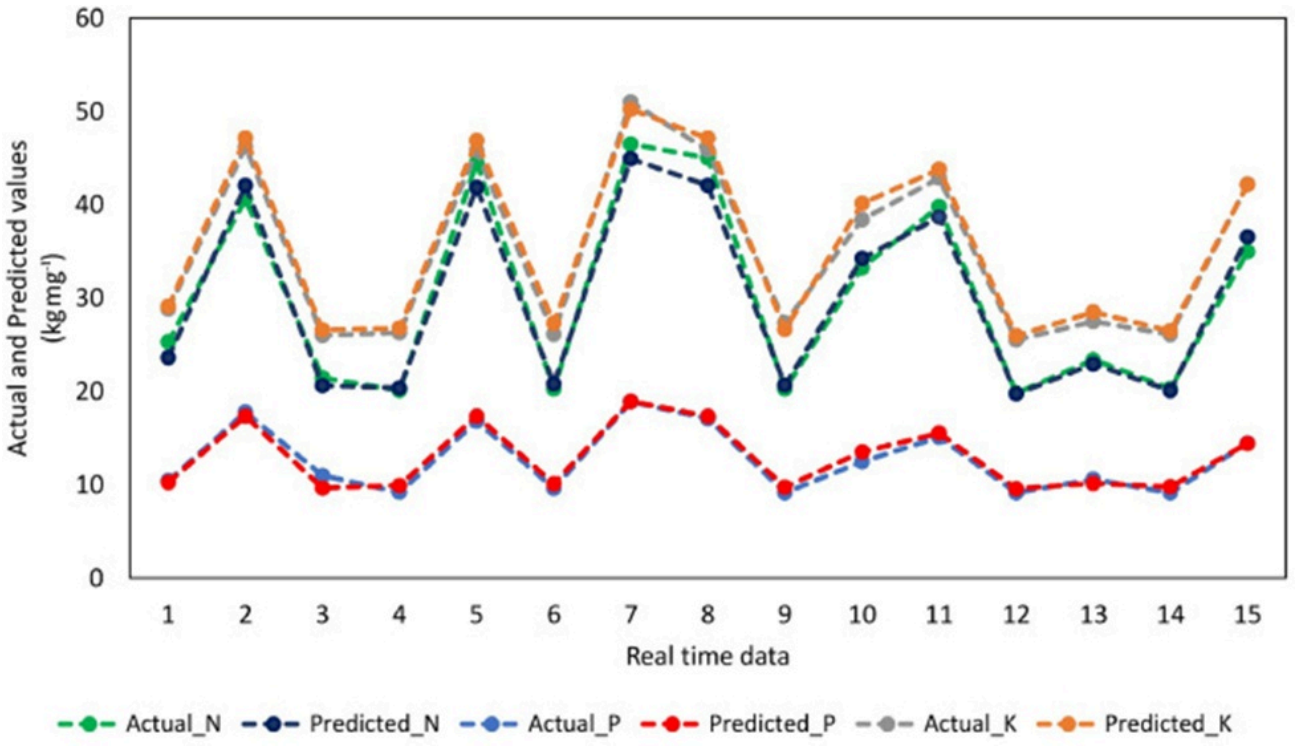

Figure 13. Validation plot of the developed tool based on real-time data.

Conclusion

Previous research programs have sought to generate predictions for cabbage and other horticultural commodities using various machine learning methods. Nevertheless, a pronounced deficiency within the extant scholarly corpus has been diagnosed: namely, the pervasive absence of lucid, human-comprehensible accounts explicating the inferential mechanisms through which such prognostications are derived. The emergence of explainable artificial intelligence as a distinct disciplinary thrust was spurred precisely by the imperative to demystify model-generated outputs. The investigation reported herein successfully demonstrated the coupled tasks of forecasting and subsequently illuminating the edaphic reservoirs of N, P, and K in concert with observable cabbage developmental traits. To operationalize this dual mandate, the interpretability frameworks SHAP and LIME were employed, with SHAP providing a synoptic, population-level perspective and LIME offering fine-grained, instance-specific decompositions. An initial round of comparative model triage established the ANN architecture as the preeminent candidate for the predictive undertaking, a determination underwritten by its markedly superior performance metrics: appreciably compressed MSE readings (Training = 1.82, Testing = 1.18) and elevated R^2 indices (Training = 0.96, Testing = 0.97) when benchmarked against SVR, KNN, and

© 2022 The Author(s). | Published by Agro Intelligence Research Press

Decision Tree configurations. Global feature attribution analysis conducted via SHAP brought to light the finding that certain input dimensions—prominently, the day tally and the mean foliar surface area—systematically depressed the model's N, P, and K estimates, whereas alternative dimensions—most conspicuously, the foliar count and the plant's vertical reach—systematically elevated them. Extending this interpretive depth, the localized dissections afforded by LIME underscored the contingent, context-dependent manner in which these same feature contributions manifested across disparate instance categories, thereby yielding a richly textured comprehension of the internal logic governing the prediction workflow. To democratize engagement with the predictive engine, a software application with an uncluttered, non-specialist interface was developed. This platform equips stakeholders endowed with heterogeneous levels of computational literacy to harness the model's inferential capabilities productively. By effectively spanning the divide between opaque, high-dimensional machine learning internals and the practical needs of terminal users, this research's contributions advance the goal of making predictive analytics broadly accessible within the agricultural sector, with potential spillover relevance to cognate fields.

Forging a linkage between the predictive modeling core and Internet of Things telemetry infrastructures opens up the tantalizing prospect of uninterrupted, real-time surveillance of rhizosphere nutrient fluxes. By strategically deploying IoT-enabled edaphic sensor nodes engineered to transduce variables such as substrate moisture tension, proton activity, thermal regime, and bioavailable nutrient ionic concentrations, a continuous stream of measurements can be captured and transmitted via wireless protocols to a centralized analytical repository. Advanced computational workflows can thereafter interrogate these streaming data torrents to distill actionable management advisories, thereby facilitating precisely timed agronomic course corrections and the rationalization of amendment application schedules.

The symbiotic melding of machine learning inferential engines with IoT sensory apparatuses constitutes a paradigmatic leap forward within the precision agriculture movement. Such convergence gives rise to cognitively augmented systems possessing the twin faculties of perpetually diagnosing soil health status in situ and proactively forecasting impending nutrient depletions or surfeits through the ongoing assimilation of freshly harvested data. The prospective dividends of these tightly integrated cyber-physical systems encompass markedly improved input utilization efficiency, a contracted ecological footprint attributable to more targeted agrochemical deployment, and a tangible uplift in harvested biomass yields.

Acknowledgements

None

Conflict of interest

None

Financial support

None

Ethics statement

None

Received: 16 Sep 2021 Revised: 21 Nov 2021 Accepted: 08 Dec 2021
Published online: 25 May 2022

© 2022 The Author(s). | Published by Agro Intelligence Research Press

Rights and permissions

Open Access The author(s) retain copyright. This article is licensed under the Creative Commons Attribution-NonCommercial-ShareAlike 4.0 International License. It may be shared and adapted for non-commercial purposes with appropriate attribution, an indication of changes, and distribution of adaptations under the same license. Third-party material may be subject to separate terms identified in its credit line. View the license at https://creativecommons.org/licenses/by-nc-sa/4.0/.

References

1. Sajindra H, Abekoon T, Jayakody JADCA, Rathnayake U. A novel deep learning model to predict the soil nutrient levels (N, P, and K) in cabbage cultivation. Smart Agric Technol. 2024;7:100395.

2. Saganuwan SA, Samuel A Junior, Tsekohol AS, Wanmi N. Acute toxicity study, haematological, biochemical and histopathological effects of Brassica oleracea var. capitata, Allium porrum and Cucurbita maxima in Rattus norvegicus. RPS Pharm Pharmacol Rep. 2023;2.

3. Zayed A, Sheashea M, Kassem IAA, Farag MA. Red and white cabbages: An updated comparative review of bioactives, extraction methods, processing practices, and health benefits, Crit. Rev Food Sci Nutr. 2022;63: 7025–42.

4. Uuh-Narvaez JJ, Segura-Campos MR. Cabbage (Brassica oleracea var. capitata): a food with functional properties aimed to type 2 diabetes prevention and management. J Food Sci. 2021;86:4775–98. https://doi.org/10.1111/1750-3841.15939.

5. Xu Y, Xiao Y, Lagnika C, Li D, Liu C, Jiang N, et al. A comparative evaluation of nutritional properties, antioxidant capacity and physical characteristics of cabbage (Brassica oleracea var. Capitate var L.) subjected to different drying methods. Food Chem. 2020;309:124935. https://doi.org/10.1016/j.foodchem.2019.06.002..

6. Rana S, Thakur KS, Bhardwaj RK, Kansal S, Sharma R. Effect of biofertilizers and micronutrients on growth and quality attributes of cabbage (Brassica oleracea var. capitata L.). Int J Chem Stud. 2020;8:1656–60. https://doi.org/10.22271/chemi.2020.v8.i1x.8501.

7. Moreb N, Murphy A, Jaiswal S, Jaiswal AK. Cabbage. Elsevier Ebooks. 2020:33–54.

8. Cho YH, Hong SM, Kim CH. Isolation and characterization of lactic acid bacteria from Kimchi, Korean traditional fermented food to apply into fermented dairy products. Korean J Food Sci Anim Resour. 2013;33:75–82.

9. Marasek-Ciolakowska A, Soika G, Warabieda W, Kowalska U, Rybczyński D. Investigation on the relationship between morphological and anatomical characteristic of Savoy cabbage and kale leaves and infestation by cabbage whitefly (Aleyrodes proletella L.). Agronomy. 2021;11:275. https://doi.org/10.3390/agronomy11020275.

10. Ling KF. The Food of Asia - featuring authentic recipes from Chefs. PDF Room. 2002. https://pdfroom.com/books/the-food-of-asia-featuring-authentic-recipes-from-master-chefs-kong-foong-ling/bXgPXjWAgev (accessed 3 January 2024).

11. Viña SZ, Olivera DF, Marani CM, Ferreyra RM, Mugridge A, Chaves AR, et al. Quality of Brussels sprouts (Brassica oleracea L. gemmifera DC) as affected by blanching method. J Food Eng. 2007;80:218–25. https://doi.org/10.1016/j.jfoodeng.2006.02.049.

12. Chohura P, Kołota E. Suitability of some nitrogen fertilizers for the cultivation of early cabbage. J Elementol. 2014. https://doi.org/10.5601/jelem.2014.19.3.704.

13. Chhetri RB. Effect of organic nutrients on the yield of cabbage. Bhutan J Nat Resour Dev. 2014;1:32–6.

© 2022 The Author(s). | Published by Agro Intelligence Research Press

14. Karthika KS, Philip PS, Neenu S. Brassicaceae Plants Response and Tolerance to Nutrient Deficiencies. Springer eBooks. 2020:337–62.

15. Shahena S, Rajan M, Chandran V, Mathew L. Conventional Methods of Fertilizer Release. Elsevier eBooks. 2021:1–24.

16. Moyin-Jesu EI. Use of different organic fertilizers on soil fertility improvement, growth and head yield parameters of cabbage (Brassica oleraceae L). Int J Recycl Org Waste Agric. 2015;4:291–8. https://doi.org/10.1007/s40093-015-0108-0..

17. Karunathilake EMBM, Le AT, Heo S, Chung YS, Mansoor S. The path to smart farming: innovations and opportunities in precision agriculture. Agriculture. 2023;13:1593. https://doi.org/10.3390/agriculture13081593.

18. Uttsha MM, Haque AKMN, Banna TT, Deowan SA, Islam MA, Babu HMH. Enhancing agricultural automation through weather invariant soil parameter prediction using machine learning. Heliyon. 2024;10:e28626. https://doi.org/10.1016/j.heliyon.2024.e28626.

19. Taffese WZ, Abegaz KA. Artificial intelligence for prediction of physical and mechanical properties of stabilized soil for affordable housing. Appl Sci. 2021;11:7503. https://doi.org/10.3390/app11167503.

20. Morales A, Villalobos FJ. Using machine learning for crop yield prediction in the past or the future. Front Plant Sci. 2023;14. https://doi.org/10.3389/fpls.2023.1128388.

21. Elbasi E, Zaki C, Topcu AE, Abdelbaki W, Zreikat AI, Cina E, et al. Crop prediction model using machine learning algorithms. Appl Sci. 2023;13:9288. https://doi.org/10.3390/app13169288.

22. Sajindra H, Abekoon T, Wimalasiri EM, Mehta D, Rathnayake U. An artificial neural network for predicting groundnut yield using climatic data. AgriEngineering. 2023;5:1713–36. https://doi.org/10.3390/agriengineering5040106.

23. Zhang L, Zhang L. Artificial Intelligence for Remote sensing Data analysis: a review of challenges and opportunities. IEEE Geosci Remote Sens Mag. 2022;10:270–94. https://doi.org/10.1109/mgrs.2022.3145854.

24. Ai S, Guo R, Liu B, Ren L, Naeem S, Zhang W, et al. A field study on the dynamic uptake and transfer of heavy metals in Chinese cabbage and radish in weak alkaline soils. Environ Sci Pollut Res Int. 2016;23:20719–27. https://doi.org/10.1007/s11356-016-7277-x.

25. Choi YO, Lee J, Sim JH, Lee SW. Development of a modified model for predicting cabbage yield based on soil properties using GIS. J Korean Soc Surv Geod Photogramm Cartogr. 2022;40:449–56.

26. Ekanayake IU, Meddage DPP, Rathnayake U. A novel approach to explain the black-box nature of machine learning in compressive strength predictions of concrete using Shapley additive explanations (SHAP). Case Stud Constr Mater. 2022;16:e01059. https://doi.org/10.1016/j.cscm.2022.e01059..

27. Hassija V, Chamola V, Mahapatra A, Singal A, Goel D, Huang K, et al. Interpreting black-box models: A review on explainable artificial intelligence. Cognit Comput. 2023;16:45–74. https://doi.org/10.1007/s12559-023-10179-8..

© 2022 The Author(s). | Published by Agro Intelligence Research Press

28. Kenny EM, Ford C, Quinn M, Keane MT. Explaining black-box classifiers using post-hoc explanations-by-example: the effect of explanations and error-rates in XAI user studies. Artif Intell. 2021;294:103459. https://doi.org/10.1016/j.artint.2021.103459.

29. Guindo ML, Kabir MH, Chen R, Huang J, Liu F, Li X, et al. Chemometric approach based on explainable AI for rapid assessment of macronutrients in different organic fertilizers using fusion spectra. Molecules. 2023;28:799. https://doi.org/10.3390/molecules28020799.

30. Gwiazdowska D, Juś K, Jasnowska-Małecka J, Kluczyńska K. The impact of polyphenols on bifidobacterium growth. Acta Biochim Pol. 2015;62:895–901. https://doi.org/10.18388/abp.2015_1154.

31. Suman RR, Mall R, Sukumaran S, Satpathy M. Extracting state models for Black-Box software components. J Object Technol. 2010;9:79. https://doi.org/10.5381/jot.2010.9.3.a3..

32. Adadi A, Berrada M. Peeking inside the Black-box: a survey on explainable artificial intelligence (XAI). IEEE Access. 2018;6:52138–60. https://doi.org/10.1109/access.2018.2870052.

33. Ehsan U, Liao QV, Muller M, Riedl MO, Weisz JD. Expanding explainability: towards social transparency in AI systems. CHI Conf Human Factor Comput Syst. 2021.

34. Tocchetti A, Brambilla M. The role of human knowledge in explainable AI. Data. 2022;7:93. https://doi.org/10.3390/data7070093.

35. Department of Census and Statistics. http://www.statistics.gov.lk/. (accessed 4 January 2024).

36. Rajapaksha L, Gunathilake DC, Pathirana S, Fernando T. Reducing post-harvest losses in fruits and vegetables for ensuring food security – Case of Sri Lanka. MOJ Food Process Technol. 2021;9:7–16. https://doi.org/10.15406/mojfpt.2021.09.00255.

37. Champa WAH, Palipane KB, Weerakkody WAP, Fernando MD. Maturity indices for harvesting of cabbage (Brassica oleraceae L.) variety green coronet. Trop Agric Res. 2007;19:254–64.

38. Weerakkody WAP, Mawalagedera SMMR. Recent Developments in Vegetable Production Technologies in Sri Lanka, Springer eBooks; 2020:189–214.

39. Marasinghe J, Karunarane SHPP, Surendran SN, Hemachandra K. Insecticide resistance, resistance mechanisms, and phylogeny of three Myzus persicae populations in cabbage from three agroclimatic zones of Sri Lanka. Trop Agric Res. 2023;34:80–93.

40. Apolo-Apolo OE, Pérez-Ruiz M, Martínez-Guanter J, Egea G. A mixed data-based deep neural network to estimate leaf area index in wheat breeding trials. Agronomy. 2020;10:175. https://doi.org/10.3390/agronomy10020175.

41. Yeshitila M, Taye M. Non-destructive prediction models for estimation of leaf area for most commonly grown vegetable crops in Ethiopia. Sci J Appl Math Stat. 2016;4:202. https://doi.org/10.11648/j.sjams.20160405.13.

42. Sharifzadeh M, Sikinioti-Lock A, Shah N. Machine-learning methods for integrated renewable power generation: a comparative study of artificial neural networks, support vector regression, and Gaussian Process regression. Renew Sustain Energy Rev. 2019;108:513–38. https://doi.org/10.1016/j.rser.2019.03.040.

© 2022 The Author(s). | Published by Agro Intelligence Research Press

43. Ayodeji A, Liu YK. SVR optimization with soft computing algorithms for incipient SGTR diagnosis. Ann Nucl Energy. 2018;121:89–100. https://doi.org/10.1016/j.anucene.2018.07.011.

44. Shafizadeh-Moghadam H, Tayyebi A, Ahmadlou M, Delavar MR, Hasanlou M. Integration of genetic algorithm and multiple kernel support vector regression for modeling urban growth. Comput Environ Urban Syst. 2017;65:28–40. https://doi.org/10.1016/j.compenvurbsys.2017.04.011..

45. Jeng NJT. Hybrid approach of selecting hyperparameters of support vector machine for regression. IEEE Trans Syst Man Cybern. 2006;36:699–709. https://doi.org/10.1109/tsmcb.2005.861067.

46. Zhang Z, Gao G, Tian Y, Yue J. Two-phase multi-kernel LP-SVR for feature sparsification and forecasting. Neurocomputing. 2016;214:594–606. https://doi.org/10.1016/j.neucom.2016.06.049..

47. Suyal M, Goyal P. A review on analysis of K-nearest neighbor classification machine learning algorithms based on supervised learning. Int J Eng Trends Technol. 2022;70:43–8. https://doi.org/10.14445/22315381/ijett-v70i7p205.

48. Steinbach M, Tan PN. kNN: k-nearest neighbors. In: The Top Ten Algorithms in Data Mining. Chapman and Hall/CRC. 2009:165–76.

49. Alfeilat HAA, Hassanat ABA, Lasassmeh O, Tarawneh AS, Alhasanat MB, Salman HSE, et al. Effects of distance measure choice on K-nearest neighbor classifier performance: a review. Big Data. 2019;7:221–48. https://doi.org/10.1089/big.2018.0175.

50. Imandoust SB, Bolandraftar M. Application of k-nearest neighbor (kNN) approach for predicting economic events. theoretical background. Int J Eng Res Appl. 2013;3:605–10.

51. Strobl C, Boulesteix AL, Augustin T. Unbiased split selection for classification trees based on the Gini Index. Comput Stat Data Anal. 2007;52:483–501. https://doi.org/10.1016/j.csda.2006.12.030..

52. De Ville B. Decision trees. Wiley Interdiscip Rev Comput Stat. 2013;5:448–55. https://doi.org/10.1002/wics.1278.

53. Esposito F, Malerba D, Semeraro G, Kay J. A comparative analysis of methods for pruning decision trees. IEEE Trans Pattern Anal Mach Intell. 1997;19:476–93. https://doi.org/10.1109/34.589207.

54. Agatonovic-Kustrin S, Beresford R. Basic concepts of artificial neural network (ANN) modeling and its application in pharmaceutical research. J Pharm Biomed Anal. 2000;22:717–27. https://doi.org/10.1016/S0731-7085(99)00272-1.

55. Azadeh A, Maghsoudi A, Sohrabkhani S. An integrated artificial neural networks approach for predicting global radiation. Energy Convers Manage. 2009;50:1497–505. https://doi.org/10.1016/j.enconman.2009.02.019.

56. Abekoon T, Buthpitiya BLSK, Sajindra H, Samarakoon ERJ, Jayakody JADCA, Kantamaneni K, et al. A comprehensive review to evaluate the synergy of intelligent food packaging with modern food technology and artificial intelligence field. Discover Sustain. 2024;5. https://doi.org/10.1007/s43621-024-00371-7.

© 2022 The Author(s). | Published by Agro Intelligence Research Press

57. Abekoon T, Sajindra H, Jayakody JADCA, Samarakoon ERJ, Rathnayake U. Image processing techniques to identify tomato quality under market conditions. Smart Agric Technol. 2024;7:100433. https://doi.org/10.1016/j.atech.2024.100433.

58. Baskin II, Winkler D, Tetko IV. A renaissance of neural networks in drug discovery. Expert Opin Drug Discov. 2016;11:785–95. https://doi.org/10.1080/17460441.2016.1201262.

59. Pradhan B, Lee S. Landslide susceptibility assessment and factor effect analysis: backpropagation artificial neural networks and their comparison with frequency ratio and bivariate logistic regression modelling. Environ Modell Softw. 2010;25:747–59. https://doi.org/10.1016/j.envsoft.2009.10.016.

60. Hasan MdM. Understanding model predictions: A comparative analysis of SHAP and LIME on various ML algorithms. J Sci Technol Res. 2024;5:17–26. https://doi.org/10.59738/jstr.v5i1.23(17-26).eaqr5800.

61. Lundberg SM, Lee SI. A unified approach to interpreting model predictions. Adv Neural Inf Process Syst. 2017;30.

62. Meddage P, Ekanayake I, Perera US, Azamathulla HMd, Md Said MA, Rathnayake U. Interpretation of machine-learning-based (black-box) wind pressure predictions for low-rise gable-roofed buildings using Shapley additive explanations (SHAP). Buildings. 2022;12:734. https://doi.org/10.3390/buildings12060734..

63. Parsa AB, Movahedi A, Taghipour H, Derrible S, Mohammadian A. Toward safer highways, application of XGBoost and SHAP for real-time accident detection and feature analysis. Accident Anal Prev. 2020;136:105405. https://doi.org/10.1016/j.aap.2019.105405.

64. Yap M, Johnston RL, Foley H, MacDonald S, Kondrashova O, Tran KA, et al. Verifying explainability of a deep learning tissue classifier trained on RNA-seq data. Sci Rep. 2021;11:1–2.

65. Liang Y, Li S, Yan C, Li M, Jiang C. Explaining the black-box model: a survey of local interpretation methods for deep neural networks. Neurocomputing. 2021;419:168–82. https://doi.org/10.1016/j.neucom.2020.08.011..

66. Madhushani C, Dananjaya K, Ekanayake IU, Meddage DPP, Kantamaneni K, Rathnayake U. Modeling streamflow in non-gauged watersheds with sparse data considering physiographic, dynamic climate, and anthropogenic factors using explainable soft computing techniques. J Hydrol. 2024;631:130846. https://doi.org/10.1016/j.jhydrol.2024.130846..

67. Mamalakis A, Barnes EA, Ebert-Uphoff I. Carefully choose the baseline: lessons learned from applying XAI attribution methods for regression tasks in geoscience. Artif Intell Earth Syst. 2023;2.

68. Nguyen HTT, Cao HQ, Nguyen KVT, Pham NDK. Evaluation of explainable artificial intelligence: SHAP, LIME, and CAM. Proc FPT AI Conf. 2021:1–6.

69. Ribeiro MT, Singh S, Guestrin C. Why should I trust you? Proceedings of the 22nd ACM SIGKDD International Conference on Knowledge Discovery and Data Mining. 2016. https://doi.org/10.1145/2939672.2939778.

70. Wieland R, Lakes T, Nendel C. Using Shapley additive explanations to interpret extreme gradient boosting predictions of grassland degradation in Xilingol, China. Geosci Model Dev. 2021;14:1493–510. https://doi.org/10.5194/gmd-14-1493-2021..

71. Zhang D. A coefficient of determination for generalized linear models. Am Stat. 2017;71:310–6. https://doi.org/10.1080/00031305.2016.1256839.

© 2022 The Author(s). | Published by Agro Intelligence Research Press

72. Zafar MR, Khan N. Deterministic local interpretable model-agnostic explanations for stable explainability. Mach Learn Knowl Extr. 2021;3:525–41. https://doi.org/10.3390/make3030027..

© 2022 The Author(s). | Published by Agro Intelligence Research Press